

## 9 Gaussian Beam Theory and Transducer Modeling

As seen in the last Chapter and in Appendix D plane waves and spherical waves are important wave types. They can be used as a means to understand many aspects of wave propagation and scattering and they can serve as building blocks to form more complex waves such as the beam of ultrasound generated by an ultrasonic transducer. As building blocks, however, plane waves and spherical waves have some disadvantages. To adequately represent the high frequency beams found in ultrasonic NDE applications, many plane wave components or spherical wave sources are needed, leading to computational inefficiencies. Also, as discussed in the last Chapter, when these wave types are transmitted or reflected through certain geometries at high frequencies mathematical singularities in the resulting approximate wave fields can be encountered that must be eliminated. These wave types do have the virtue of being exact solutions to the equations of motion for both fluids and solids so that other wave fields formed from them also satisfy the equations of motion exactly as long as the wave fields are not obtained with the use of approximations.

Gaussian beams are another important wave type that can eliminate many of the disadvantages of plane waves and spherical waves. In this Chapter we will show that it is possible to accurately model the sound beam of an ultrasonic transducer with as few as ten Gaussian beams. Furthermore, we will see that it is possible to analytically define the propagation and transmission/reflection laws for these Gaussian beams even after they have undergone multiple interactions with curved interfaces. These properties of Gaussian beams will allow us to construct a multi-Gaussian transducer beam model that is computationally efficient and capable of simulating sound beams generated in very complex inspection geometries. Unlike plane waves and spherical waves, Gaussian beams are only approximate paraxial solutions to the governing equations of motion. Similarly, a multi-Gaussian transducer beam model will also be an approximate paraxial solution. Thus, there will be some situations where a multi-Gaussian beam model will lose accuracy. We will describe those special cases in some detail later. Fortunately, many of those special cases

are not encountered in common testing setups so a multi-Gaussian beam model is a practical, powerful modeling tool for many NDE applications.

In Appendix F we have given an extensive discussion of Gaussian beam fundamentals for the special case of circularly symmetrical Gaussian beams to illustrate the important properties of Gaussian beams in a simple context. While circularly symmetrical Gaussian beams are very useful for describing many laser science problems, they are of limited use for the types of problems we need to model in ultrasonic inspections. In this Chapter we extend the treatment given in Appendix F to the more general Gaussian beams that are needed for ultrasonic NDE applications.

### 9.1 The Paraxial Wave Equation and Gaussian Beams in a Fluid

Consider first the case of wave propagation in a fluid. We know that the pressure,  $p$ , satisfies the wave equation. If we place a harmonic wave solution (of  $\exp(-i\omega t)$  time dependency) into the wave equation in the form of a quasi-plane wave traveling in the  $x_3$ -direction given by:

$$p = P(x_1, x_2, x_3) \exp(ik_p x_3) \quad (9.1)$$

(Note - we will not write the time dependency explicitly here or in most subsequent expressions) then we find that  $P$  satisfies the equation

$$\frac{\partial^2 P}{\partial x_1^2} + \frac{\partial^2 P}{\partial x_2^2} + \frac{\partial^2 P}{\partial x_3^2} + 2ik_p \frac{\partial P}{\partial x_3} = 0. \quad (9.2)$$

If we use the solution of Eq. (9.1) to represent a wave which is propagating primarily in the  $x_3$ -direction, then we expect that at high frequencies the complex exponential term in Eq. (9.1) will capture most of the wave field variations in the  $x_3$ -coordinate so that the wave diffraction effects associated with the  $\partial^2 P / \partial x_3^2$  term in Eq. (9.2) will be small in comparison to all the other terms in that equation, i.e. we make the *paraxial approximation* [9.1]

$$\frac{\partial^2 P}{\partial x_3^2} \ll \frac{\partial^2 P}{\partial x_1^2}, \frac{\partial^2 P}{\partial x_2^2}, 2ik_p \frac{\partial P}{\partial x_3} \quad (9.3)$$

which leads to the *paraxial wave equation* for  $P$ :

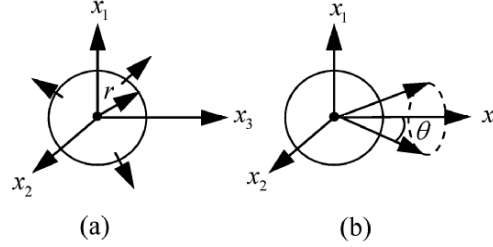


**Fig. 9.1.** (a) Propagation of a spherical wave from a point source and (b) the behavior of the spherical wave in a small region around the  $x_3$ -axis.

$$\frac{\partial^2 P}{\partial x_1^2} + \frac{\partial^2 P}{\partial x_2^2} + 2ik_p \frac{\partial P}{\partial x_3} = 0. \quad (9.4)$$

In Appendix F it is shown that the paraxial approximation of Eq. (9.3) places some physical limits on the properties of a propagating Gaussian beam.

We can also gain some physical understanding of the meaning of the paraxial approximation by considering the radiation of a spherical wave from a point source in a fluid as shown in Fig. 9.1 (a). The pressure in the fluid in this spherical wave is given by

$$p = A \frac{\exp(ik_p r)}{r}, \quad (9.5)$$

where  $r = \sqrt{x_1^2 + x_2^2 + x_3^2}$  is the radial distance from the source and  $k_p = \omega/c_p$  is the wave number, with  $\omega$  the frequency in radians/sec and  $c_p$  the wave speed of the fluid.

Now, consider this spherical wave in the neighborhood of a fixed direction, which we will take as the  $x_3$ -axis (see Fig. 9.1 (b)). In a small angular region about this axis (where  $x_1/x_3 \ll 1, x_2/x_3 \ll 1$ ) the spherical wave is traveling approximately in the  $x_3$ -direction and we have  $r = \sqrt{x_3^2 + \rho_0^2} \cong x_3 + \rho_0^2/2x_3$ , where  $\rho_0 = \sqrt{x_1^2 + x_2^2}$ . In this case, the spherical wave can be approximated by

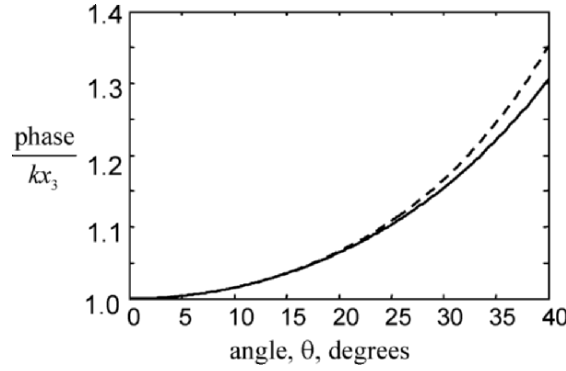


**Fig. 9.2.** Normalized phase for a spherical wave in the neighborhood of the  $x_3$ -axis. Solid line: exact normalized phase, dashed line: paraxial approximation for the normalized phase.

$$p \cong A \frac{\exp\left[ik_p \left(x_3 + \rho_0^2 / 2x_3\right)\right]}{x_3}, \quad (9.6)$$

which satisfies the paraxial wave equation exactly so that Eq. (9.6) is the paraxial approximation of the spherical wave in the neighborhood of the  $x_3$ -axis. How large of an angular neighborhood about the  $x_3$ -axis can we take before the paraxial approximation loses accuracy in describing the spherical wave? To answer this question, consider the phase term of the spherical wave ( $k_p r$ ) divided by the phase of a plane wave traveling in the  $x_3$ -direction ( $k_p x_3$ ) and let  $\rho_0 / x_3 = \tan(\theta)$ , where  $\theta$  defines an angle about the  $x_3$ -axis (Fig. 9.1(b)). [Remark - a normalized phase term is considered here so that we can discuss phase differences in non-dimensional terms and we consider the phase differences, not the amplitude differences since it is the former that are most sensitive to approximation] Then we have:

$$\text{exact spherical wave:} \quad \frac{k_p r}{k_p x_3} = \sqrt{1 + \tan^2 \theta} \quad (9.7a)$$

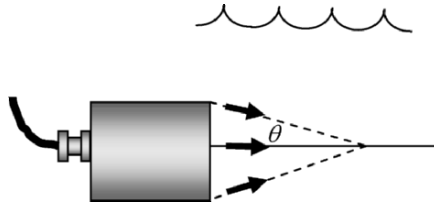
paraxial approximation: 
$$\frac{k_p r}{k_p x_3} \cong 1 + \frac{\tan^2 \theta}{2} \quad (9.7b)$$

Figure 9.2 compares these two normalized phase terms versus  $\theta$  where the solid line is the exact phase result and the dashed line is the paraxial approximation to this phase. As can be seen from that figure, the paraxial approximation for the phase begins to lose accuracy at an angle of approximately 30 degrees from the  $x_3$ -axis.

Now, apply the results for this simple example to the case of Fig. 9.3 where a planar piston transducer radiates waves into water that travel from the transducer surface to a point on the transducer axis. As discussed in the last Chapter a Rayleigh-Sommerfeld integral model represents this transducer as a distribution of point sources over the face of the transducers, each of which generates a spherical wave of the type just discussed. Thus, if we apply the paraxial approximation to those distributed sources, we would expect that the paraxial approximation for the Rayleigh-Sommerfeld model also breaks down if the angle  $\theta$  shown in Fig. 9.3 exceeds approximately 30 degrees. Typically, this means that the paraxial approximation should begin to lose accuracy when the distance from the face of the transducer to the point where the wave field being evaluated is less than about a transducer diameter. This can be demonstrated by comparing the magnitude of the exact on-axis pressure for a circular planar piston transducer radiating into a fluid, as found in Eq. (8.20):

$$p(z, \omega) = \rho c v_0 \left[ \exp(ik_p z) - \exp\left(ik_p \sqrt{a^2 + z^2}\right) \right] \quad (9.8)$$

with the same pressure in the paraxial approximation given by Eq. (8.22):



**Fig. 9.3.** A transducer radiating into a fluid.

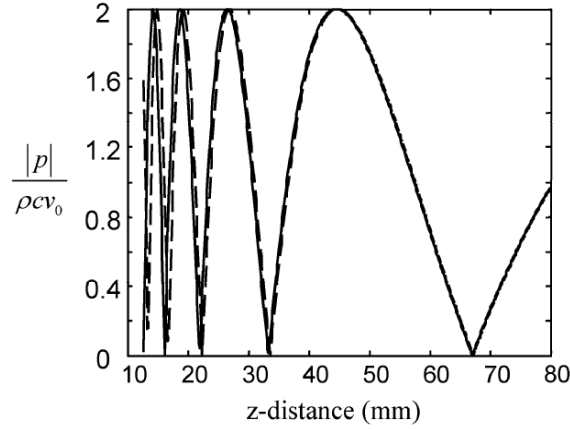


**Fig. 9.4.** A comparison of the magnitude of the normalized pressure versus on-axis  $z$ -distance for a 12.7 mm diameter, 5 MHz planar piston transducer radiating into water where the solid line is for the exact results and the dashed line is for the paraxial result.

$$p(z, \omega) \cong \rho c v_0 \exp(ik_p z) \left[ 1 - \exp(ik_p a^2 / 2z) \right]. \quad (9.9)$$

Figure 9.4 plots the magnitude of these exact and approximate pressures versus  $z$  for the case of a 5MHz, 12.7 mm diameter transducer radiating into water. It can be seen from that figure that even in the near field, where there are significant pressure variations, the paraxial approximation represents the pressure of this transducer very well but that the approximation begins to have a significant shift from the exact on-axis pattern at about one diameter distance from the transducer which is the smallest distance plotted in Fig. 9.4. This distance corresponds to an angle  $\theta$  in Fig. 9.3 of 30 degrees.

Another way of viewing the paraxial approximation of Eq. (9.3) is to recall from the last Chapter that we can also use an angular spectrum of plane waves to represent the sound beam of a transducer. Thus, consider a plane wave component of this spectrum that is traveling in the  $x_1 - x_3$  plane at an angle  $\theta$  with respect to the  $x_3$ -axis (Fig. 9.5). This plane wave is given by

$$p = A \exp(ik_p x_1 \sin \theta + ik_p x_3 \cos \theta), \quad (9.10)$$

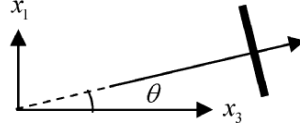


**Fig. 9.5.** A plane wave traveling in the  $x_1 - x_3$  plane at an angle  $\theta$  with respect to the  $x_3$ -axis.

which can be placed in the quasi-plane wave form of Eq. (9.1),  $p = P \exp(ik_p x_3)$ , where

$$P = A \exp[ik_p x_1 \sin \theta + ik_p x_3 (1 - \cos \theta)]. \quad (9.11)$$

Then for small angles  $\theta$

$$\begin{aligned} \frac{\partial^2 P}{\partial x_1^2} &= -k_p^2 P \sin^2 \theta \cong -k_p^2 P \theta^2 \\ 2ik_p \frac{\partial P}{\partial x_3} &= -2k_p^2 P (1 - \cos \theta) \cong k_p^2 P \theta^2 \\ \frac{\partial^2 P}{\partial x_3^2} &= -k_p^2 P (1 - \cos \theta)^2 \cong -\frac{k_p^2 P \theta^4}{4} \end{aligned} \quad (9.12)$$

so that we see that  $\partial^2 P / \partial x_3^2$  will be at least an order of magnitude smaller than the other derivative terms if  $\theta < 0.5$  rad, or approximately  $\theta < 30^\circ$ . This shows that as long as the transducer beam is sufficiently well collimated so that the angular plane wave spectrum components needed to represent the beam are very small outside a cone angle of about 30 degrees about the  $x_3$ -axis, we expect the paraxial approximation will be valid.

There are number of exact solutions to the paraxial wave equation, Eq. (9.4). An ordinary plane wave where  $P = A = \text{constant}$  is a solution. Also, as mentioned previously, the paraxial approximation of a spherical wave given by Eq. (9.6) is

$$P = A \frac{\exp[ik_p \rho_0^2 / 2x_3]}{x_3}, \quad (9.13)$$

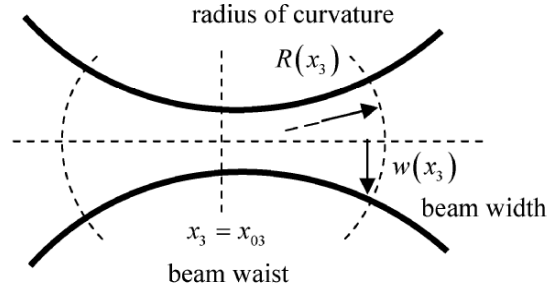


**Fig. 9.6.** A Gaussian beam of circular cross-section propagating in the  $x_3$ -direction, showing the wave front curvature and the beam width. The beam waist is located at  $x_3 = x_{03}$ .

which is an exact solution of the paraxial wave equation. We can also obtain a solution of Eq. (9.4) in the form of a Gaussian beam propagating along the  $x_3$ -axis. Here, we will consider a general form of a Gaussian beam given by:

$$P = P(x_3) \exp\left(\frac{i\omega}{2} \mathbf{X}^T \mathbf{M}_p(x_3) \mathbf{X}\right), \quad \mathbf{X} = [x_1, x_2]^T \quad (9.14)$$

where  $P(x_3)$  is a complex-valued scalar, and  $\mathbf{M}_p$  is a  $2 \times 2$  complex-valued symmetric matrix. A circular cross-section Gaussian beam of the type considered in Appendix F is then a special case of Eq. (9.14). This type of Gaussian beam is shown schematically in Fig. 9.6 along with some of its defining parameters (beam width, radius of curvature). For an in-depth discussion of these and other defining parameters, see Appendix F. We will also discuss later in this Chapter how the  $\mathbf{M}_p$  matrix is related to these properties of the propagating beam. Substituting Eq. (9.14) into Eq. (9.4), we obtain

$$\frac{2}{c_p} \frac{dP}{dx_3} + P \operatorname{tr}(\mathbf{M}_p) + i P \mathbf{X}^T \left( \frac{1}{c_p} \frac{d\mathbf{M}_p}{dx_3} + \mathbf{M}_p^2 \right) \mathbf{X} = 0. \quad (9.15)$$

In order to satisfy Eq. (9.15) for all  $\mathbf{X}$ , we obtain the two equations

$$\frac{2}{c_p} \frac{dP}{dx_3} + P \operatorname{tr}(\mathbf{M}_p) = 0 \quad (9.16)$$



and

$$\frac{1}{c_p} \frac{d\mathbf{M}_p}{dx_3} + \mathbf{M}_p^2 = 0, \quad (9.17)$$

where  $\text{tr}(\mathbf{M}_p)$  is the trace of the matrix  $\mathbf{M}_p$ . In ray theory, Eq. (9.16) is usually called the *transport equation* [9.2]. Equation (9.17) is in the form of a non-linear matrix *Ricatti equation* [9.2].

We can manipulate both of these equations into alternative forms where we can solve them directly. Consider first Eq. (9.17). We start by differentiating the identity  $\mathbf{M}_p \mathbf{M}_p^{-1} = \mathbf{I}$  with respect to  $x_3$ . We obtain

$$\left( \frac{d\mathbf{M}_p}{dx_3} \right) \mathbf{M}_p^{-1} + \mathbf{M}_p \left( \frac{d\mathbf{M}_p^{-1}}{dx_3} \right) = 0. \quad (9.18)$$

If we use Eq. (9.17) in this result and pre-multiply by  $\mathbf{M}_p^{-1}$ , then we obtain

$$\frac{d\mathbf{M}_p^{-1}}{dx_3} - c_p \mathbf{I} = 0, \quad (9.19)$$

where  $\mathbf{I}$  is the  $2 \times 2$  identity matrix. Equation (9.19) gives us a simple differential relationship that we will use shortly to obtain the solution of Eq. (9.17). Now, consider transforming the  $\mathbf{M}_p$  part of Eq. (9.16). If we pre-multiply Eq. (9.19) by  $\mathbf{M}_p$  we find

$$\mathbf{M}_p = \frac{1}{c_p} \mathbf{M}_p \left( \frac{d\mathbf{M}_p^{-1}}{dx_3} \right). \quad (9.20)$$

Using the relationship

$$\mathbf{M}_p = \left( \mathbf{M}_p^{-1} \right)^{-1} = \frac{\text{adj}(\mathbf{M}_p^{-1})}{\det(\mathbf{M}_p^{-1})} \quad (9.21)$$

(which comes directly from the definition of the inverse of a matrix) in Eq. (9.20) yields

$$\mathbf{M}_p = \frac{1}{c_p \det(\mathbf{M}_p^{-1})} \text{adj}(\mathbf{M}_p^{-1}) \left( \frac{d\mathbf{M}_p^{-1}}{dx_3} \right), \quad (9.22)$$

where  $\text{adj}[\ ]$  denotes the adjoint and  $\det[\ ]$  the determinant. Taking the trace of both sides of Eq. (9.22) and applying the general matrix relationship [9.3]

$$\frac{d[\det(\mathbf{M}_p^{-1})]}{dx_3} = \text{tr}[\text{adj}(\mathbf{M}_p^{-1})(d\mathbf{M}_p^{-1}/dx_3)], \quad (9.23)$$

it follows that

$$\begin{aligned} \text{tr}(\mathbf{M}_p) &= \frac{1}{c_p \det(\mathbf{M}_p^{-1})} \frac{d[\det(\mathbf{M}_p^{-1})]}{dx_3} \\ &= \frac{1}{c_p} \frac{d\{\ln[\det(\mathbf{M}_p^{-1})]\}}{dx_3}. \end{aligned} \quad (9.24)$$

Placing Eq. (9.24) into Eq. (9.16) then gives

$$2 \frac{dP}{dx_3} + P \frac{d}{dx_3} [\ln(\det[\mathbf{M}_p^{-1}])] = 0. \quad (9.25)$$

The solutions of Eqs. (9.19) and (9.25) are now both easy to obtain. The solution of Eq. (9.19) by direct integration gives us the *propagation law*:

$$\begin{aligned} \mathbf{M}_p^{-1}(x_3) &= c_p x_3 \mathbf{I} + \mathbf{M}_p^{-1}(0) \\ &= [c_p x_3 \mathbf{M}_p(0) + \mathbf{I}] \mathbf{M}_p^{-1}(0). \end{aligned} \quad (9.26)$$

Taking the inverse of both sides of Eq. (9.26) gives the corresponding solution for  $\mathbf{M}_p$ :

$$\mathbf{M}_p(x_3) = \mathbf{M}_p(0) [\mathbf{I} + c_p x_3 \mathbf{M}_p(0)]^{-1}, \quad (9.27)$$

which can be rewritten as

$$\mathbf{M}_p(x_3) = \frac{1}{\Delta} (\mathbf{M}_p(0) + x_3 c_p \mathbf{I} \det[\mathbf{M}_p(0)]) \quad (9.28)$$

where

$$\Delta = 1 + (x_3 c_p) \text{tr}[\mathbf{M}_p(0)] + (x_3 c_p)^2 \det[\mathbf{M}_p(0)]. \quad (9.29)$$

The solution of Eq. (9.25) also follows directly, since we can write it in the equivalent form

$$d \left\{ \ln \left[ \frac{P(x_3)}{P(0)} \right] \right\} / dx_3 = d \left\{ \ln \left[ \det \left( \frac{\mathbf{M}_p^{-1}(x_3)}{\mathbf{M}_p^{-1}(0)} \right)^{-1/2} \right] \right\} / dx_3, \quad (9.30)$$

where  $P(0)$  is  $P(x_3)|_{x_3=0}$ . Equation (9.30) can then also be integrated, leading to any one of the following equivalent forms:

$$\begin{aligned} \frac{P(x_3)}{P(0)} &= \sqrt{\frac{\det[\mathbf{M}_p^{-1}(0)]}{\det[\mathbf{M}_p^{-1}(x_3)]}} = \sqrt{\frac{\det[\mathbf{M}_p(x_3)]}{\det[\mathbf{M}_p(0)]}} \\ &= \frac{1}{\sqrt{\det[\mathbf{I} + c_p x_3 \mathbf{M}_p(0)]}}. \end{aligned} \quad (9.31)$$

Using the second of these forms our Gaussian beam solution for the pressure,  $p$ , then can be written as

$$\begin{aligned} p(\mathbf{x}, \omega) &= P(0) \exp(ik_p x_3) \sqrt{\frac{\det[\mathbf{M}_p(x_3)]}{\det[\mathbf{M}_p(0)]}} \\ &\quad \cdot \exp\left(\frac{i\omega}{2} \mathbf{X}^T \mathbf{M}_p(x_3) \mathbf{X}\right) \end{aligned} \quad (9.32)$$

with  $\mathbf{X} = [x_1, x_2]^T$ , which shows that both the amplitude and phase of the Gaussian beam are functions solely of the matrix  $\mathbf{M}_p(x_3)$  and the starting values  $P(0), \mathbf{M}_p(0)$  at  $x_3 = 0$ . The velocity in the Gaussian beam can also be obtained by differentiating this pressure. However, in the paraxial approximation the dominant term in such a differentiation comes from the  $\exp(ik_p x_3)$  term so that the velocity is simply given by

$$\begin{aligned} \mathbf{v}^p(\mathbf{x}, \omega) &= V^p(0) \mathbf{d}^p \exp(ik_p x_3) \sqrt{\frac{\det[\mathbf{M}_p(x_3)]}{\det[\mathbf{M}_p(0)]}} \\ &\quad \cdot \exp\left(\frac{i\omega}{2} \mathbf{X}^T \mathbf{M}_p(x_3) \mathbf{X}\right), \end{aligned} \quad (9.33)$$

where  $V^p(0) = P(0)/\rho c_p$ ,  $\rho$  is the density of the fluid and  $\mathbf{d}^p$  is a unit vector in the  $x_3$ -direction (the direction of propagation). For a proof that

the other terms obtained when differentiating the pressure to obtain the velocity are indeed negligible, see the discussion in Appendix F leading up to Eq. (F.25).

Gaussian beams are often used to also represent the light beam in a laser. In the laser field the matrix  $\mathbf{M}_p$  is usually taken to be a diagonal matrix of the form (see Appendix F and [9.1])

$$\mathbf{M}_p(x_3) = \begin{bmatrix} \frac{1}{c_p q(x_3)} & 0 \\ 0 & \frac{1}{c_p q(x_3)} \end{bmatrix}, \quad (9.34)$$

where  $q(x_3)$  is a complex scalar. In this case Eq. (9.32) becomes

$$p(\mathbf{x}, \omega) = P(0) \exp(ik_p x_3) \frac{q(0)}{q(x_3)} \exp\left[\frac{ik(x_1^2 + x_2^2)}{2q(x_3)}\right] \quad (9.35)$$

and the propagation law for  $\mathbf{M}_p$  (Eq. (9.26)) is simply

$$q(x_3) = q(0) + x_3. \quad (9.36)$$

Equation (9.35) represents a propagating Gaussian beam of circular cross section. As long as the imaginary part of the starting value at  $x_3 = 0$ ,  $q(0)$ , has a negative imaginary part, the propagation law shows that  $q(x_3)$  will also have a negative imaginary part so that Eq. (9.35) will represent a beam that is always localized near the axis of propagation. If we let

$$\frac{1}{q(x_3)} = \frac{1}{R(x_3)} + i \frac{\lambda}{\pi w^2(x_3)} \quad (9.37)$$

then Eq. (9.35) can be written as

$$p(\mathbf{x}, \omega) = P(0) \exp(ik_p x_3) \frac{q(0)}{q(x_3)} \cdot \exp\left[\frac{ik(x_1^2 + x_2^2)}{2R(x_3)}\right] \exp\left[-\frac{(x_1^2 + x_2^2)}{w^2(x_3)}\right] \quad (9.38)$$

which shows that  $R(x_3)$  represents a wave front radius of curvature that varies as the Gaussian beam propagates while  $w(x_3)$  represents a beam width parameter that defines the radial distance to which the beam amplitude drops by a factor  $e^{-1}$  from its on-axis value. Figure 9.6 illustrates these quantities for a propagating Gaussian beam. From the results given in Appendix F (see Eq. (F.14)) one can write down relatively simple expressions for  $R(x_3), w(x_3)$ :

$$\begin{aligned} R(x_3) &= (x_3 - x_{03}) + x_{R3}^2 / (x_3 - x_{03}) \\ w(x_3) &= w_0 \sqrt{1 + (x_3 - x_{03})^2 / x_{R3}^2}, \end{aligned} \quad (9.39)$$

where  $w_0$  is the beam width at the waist (see Fig. 9.6), located at  $x_3 = x_{03}$  and  $x_{R3} = \pi w_0^2 / \lambda$  is the *confocal parameter*, as discussed in Appendix F.

In the laser field, most of the discussion of Gaussian beams is for circular cross-section beams where Eq. (9.34) is valid. This is because in the interactions of the Gaussian light beam in a laser (reflection from mirrors, etc) the cross-section of the Gaussian beam often remains circular. Appendix F describes similar cases where a circular cross-section Gaussian beam propagates in a fluid and interacts with spherical interfaces, resulting in transmitted and reflected beams also of circular cross-section.

In NDE problems, although the Gaussians used to model a transducer may have circular cross-sections to begin with at the transducer face, after transmission and reflection from interfaces we must normally use the more general form of Eq. (9.14) and let  $\mathbf{M}_p(x_3)$  be a complex 2x2 symmetrical matrix. As long as the two eigenvalues of  $M_m^I(x_3) \equiv \text{Im}\{\mathbf{M}_p(x_3)\}$  ( $m=1,2$ ), satisfy  $M_m^I(x_3) > 0$ , where  $\text{Im}\{\}$  indicates “imaginary part of”, Eq. (9.14) will represent a wave which has an elliptical Gaussian profile with decay away from the  $x_3$  axis and hence will be a localized beam traveling along that axis. If the general Gaussian beam of Eq. (9.14) starts out at  $x_3 = 0$  with eigenvalues of  $M_m^I(0) \equiv \text{Im}\{\mathbf{M}_p(0)\}$  ( $m=1,2$ ), that satisfy  $M_m^I(0) > 0$ , then during propagation the eigenvalues of  $\text{Im}\{\mathbf{M}_p(x_3)\}$  will also satisfy  $M_m^I(x_3) > 0$  since the propagation law, Eq. (9.26), shows that only the real parts of the eigenvalues of  $\mathbf{M}_p^{-1}$  (and, hence,  $\mathbf{M}_p$ ) are affected during propagation. Thus a localized Gaussian at  $x_3 = 0$  always generates a localized propagating Gaussian beam, just as in the circular cross-section case. Note

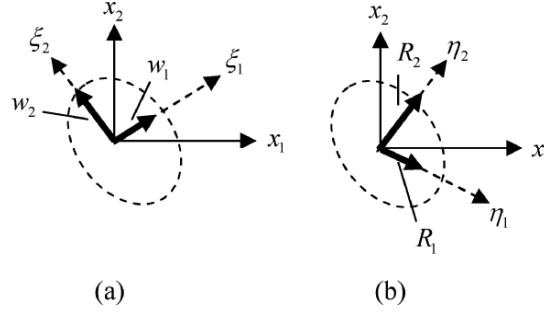


**Fig. 9.7.** The elliptical cross-section of a general propagating Gaussian beam, showing (a) the principal beam widths and principal beam width directions where the beam amplitude has fallen to  $1/e$  of its value on the beam axis, and (b) the principal wave front radii of curvatures and their directions.

that the eigenvalues of  $\text{Re}\{\mathbf{M}_p(x_3)\}$ ,  $M_m^R(x_3)$  ( $m=1,2$ ), are related to the principal wave front curvatures, where  $\text{Re}\{\}$  denotes “real part”. The directions of those principal curvatures, however, are different from the directions associated with the eigenvalues  $M_m^I(x_3)$ , which are related to the two principal beam widths for a Gaussian beam of elliptical cross-section (see Fig. 9.7). Thus, as an elliptical cross-section Gaussian beam represented by Eq. (9.32) propagates the angle between the major axes of that elliptical cross section and the principal wave front curvatures changes. If we let

$$\begin{aligned} M_m^I(x_3) &= \frac{\lambda}{\pi c_p w_m^2(x_3)} \\ M_m^R(x_3) &= \frac{1}{c_p R_m(x_3)}, \end{aligned} \quad (9.40)$$

where  $R_m, w_m$  are the principal radii of curvature and beam widths, respectively, the general Gaussian beam of Eq. (9.32) can be written as

$$\begin{aligned} p(\mathbf{x}, \omega) &= P(0) \exp(ik_p x_3) \sqrt{\frac{\det[\mathbf{M}_p(x_3)]}{\det[\mathbf{M}_p(0)]}} \\ &\cdot \exp\left[\frac{ik_p}{2} \left(\frac{\eta_1^2}{R_1} + \frac{\eta_2^2}{R_2}\right)\right] \exp\left[-\left(\frac{\xi_1^2}{w_1^2} + \frac{\xi_2^2}{w_2^2}\right)\right], \end{aligned} \quad (9.41)$$

where  $(\xi_1, \xi_2)$  and  $(\eta_1, \eta_2)$  are the principal axes for the imaginary and real parts of the  $\mathbf{M}_p$  matrix, respectively. The orientation of both these axes are functions of  $x_3$ .

Another difference between the circular cross-section case (Eq. (9.35)) and the more general case (Eq. (9.32)) is that square roots appear in the latter equation. Since the matrix  $\mathbf{M}_p$  is complex and the principal curvature and beam width directions are not aligned in general, some care must be taken in evaluating those square roots. This issue appears to have received little attention in the literature as in many Gaussian beam problems discussed the  $\mathbf{M}_p$  matrix is diagonal, i.e.

$$\mathbf{M}_p(x_3) = \begin{bmatrix} M_1(x_3) & 0 \\ 0 & M_2(x_3) \end{bmatrix}. \quad (9.42)$$

In this case it is easy to specify the roots since we can write Eq. (9.31) as

$$\frac{P(x_3)}{P(0)} = \frac{\sqrt{\det[\mathbf{M}_p(x_3)]}}{\sqrt{\det[\mathbf{M}_p(0)]}} = \frac{\sqrt{M_1(x_3)}\sqrt{M_2(x_3)}}{\sqrt{M_1(0)}\sqrt{M_2(0)}}. \quad (9.43)$$

Because the imaginary parts of  $M_m(0), M_m(x_3)$  ( $m = 1, 2$ ) are always positive, the individual square roots in Eq. (9.43) also must be taken to have positive imaginary parts.

For the more general case where  $\mathbf{M}_p$  is not diagonal, although the principal directions of the real and imaginary parts of  $\mathbf{M}_p$  do not coincide, the real part of  $\mathbf{M}_p$  is a real, symmetrical matrix and the imaginary part is a real, symmetrical and positive definite matrix. Under these conditions, matrix theory [9.5] shows that it is always possible to define a generalized eigenvalue problem where a real 2x2 transformation matrix,  $\mathbf{T}$ , can be found that *simultaneously* diagonalizes both the real and imaginary parts of  $\mathbf{M}_p$ . Knowing this transformation matrix we can then form up the term

$$\frac{\sqrt{\det[\mathbf{T}^T(x_3)\mathbf{M}_p(x_3)\mathbf{T}(x_3)]}}{\sqrt{\det[\mathbf{T}^T(0)\mathbf{M}_p(0)\mathbf{T}(0)]}} = \frac{\sqrt{\tilde{M}_1(x_3)}\sqrt{\tilde{M}_2(x_3)}}{\sqrt{\tilde{M}_1(0)}\sqrt{\tilde{M}_2(0)}} \quad (9.44)$$

and calculate the complex  $\tilde{M}_m(0), \tilde{M}_m(x_3)$  terms which are the diagonal matrix terms obtained after applying the transformation matrices to  $\mathbf{M}_p$  as

shown in Eq. (9.44). We have placed the tilde over these diagonal terms to emphasize that these complex quantities are not the same as the complex values given in Eq. (9.43). However, the square roots on the right side of Eq. (9.44) can be found in the same fashion as done with Eq. (9.43). Then in terms of the remaining real determinants, we find

$$\begin{aligned} \frac{P(x_3)}{P(0)} &= \frac{\sqrt{\det[\mathbf{M}_p(x_3)]}}{\sqrt{\det[\mathbf{M}_p(0)]}} \\ &= \frac{\sqrt{\det^2[\mathbf{T}(0)]}}{\sqrt{\det^2[\mathbf{T}(x_3)]}} \frac{\sqrt{\tilde{M}_1(x_3)}\sqrt{\tilde{M}_2(x_3)}}{\sqrt{\tilde{M}_1(0)}\sqrt{\tilde{M}_2(0)}} \end{aligned} \quad (9.45)$$

Many mathematical software packages such as MATLAB are available that obtain the transformation matrix  $\mathbf{T}$ , so that Eq. (9.45) is easy to implement in practice.

## 9.2 The Paraxial Wave Equation and Gaussian Beams in a Solid

For a homogeneous, elastic solid, the displacement potentials satisfy wave equations so that they also have paraxial Gaussian beam solutions of the form

$$\begin{aligned} \phi &= \Phi(x_3) \exp(ik_p x_3) \exp\left(\frac{i\omega}{2} \mathbf{X}^T \mathbf{M}_p(x_3) \mathbf{X}\right) \\ \psi &= \Psi(x_3) \mathbf{t} \exp(ik_s x_3) \exp\left(\frac{i\omega}{2} \mathbf{X}^T \mathbf{M}_s(x_3) \mathbf{X}\right). \end{aligned} \quad (9.46)$$

At high frequencies we can obtain the velocity,  $\mathbf{v}^\alpha$  ( $\alpha = p, s$ ), for a P-wave or S-wave by again just differentiating the  $\exp(ik_\alpha x_3)$  terms in these equations to obtain

$$\mathbf{v}^\alpha = V^\alpha(x_3) \mathbf{d}^\alpha \exp(ik_\alpha x_3) \exp\left(\frac{i\omega}{2} \mathbf{X}^T \mathbf{M}_\alpha(x_3) \mathbf{X}\right) \quad (\alpha = p, s) \quad (9.47)$$

with  $V^p = \omega^2 \Phi / c_p$ ,  $V^s = \omega^2 \Psi / c_s$  and  $\mathbf{d}^p = \mathbf{e}_3$ ,  $\mathbf{d}^s = \mathbf{e}_3 \times \mathbf{t}$ , where  $\mathbf{e}_3$  is a unit vector in the  $x_3$ -direction. Note that these relations are identical in



form to those for a plane wave since in a plane wave  $\exp(ik_\alpha x_3)$  is the only spatially varying term present.

Alternatively, we can show that a formal high frequency approximation of Navier's equations for the displacements in the quasi-plane wave form

$$u_i = \tilde{U}_i(x_1, x_2, x_3) \exp(ik_s x_3) \quad (9.48)$$

leads to the paraxial wave equation

$$\frac{\partial^2 \tilde{U}_3}{\partial x_1^2} + \frac{\partial^2 \tilde{U}_3}{\partial x_2^2} + 2ik_p \frac{\partial \tilde{U}_3}{\partial x_3} = 0 \quad (9.49)$$

with  $\tilde{U}_1 = \tilde{U}_2 = 0$  for P-waves while for S-waves

$$\frac{\partial^2 \tilde{U}_I}{\partial x_1^2} + \frac{\partial^2 \tilde{U}_I}{\partial x_2^2} + 2ik_s \frac{\partial \tilde{U}_I}{\partial x_3} = 0 \quad (I = 1, 2) \quad (9.50)$$

with  $\tilde{U}_3 = 0$  [9.6]. Since both P-waves and S-waves in a homogeneous, isotropic elastic solid satisfy paraxial equations (Eqs. (9.49) and (9.50)), elastic wave Gaussian beam solutions can be written in vector form for the displacements of both wave types as

$$\mathbf{u}^\alpha = U^\alpha(x_3) \mathbf{d}^\alpha \exp(ik_\alpha x_3) \exp\left(\frac{i\omega}{2} \mathbf{X}^T \mathbf{M}_\alpha(x_3) \mathbf{X}\right) \quad (\alpha = p, s) \quad (9.51)$$

Then Eq. (9.47) again follows, where  $\mathbf{v}^\alpha = -i\omega \mathbf{u}^\alpha$ ,  $V^\alpha(x_3) = -i\omega U^\alpha(x_3)$ .

In the solid these Gaussian beam solutions of the paraxial equation also must satisfy transport and Riccati equations given by [9.2]

$$\frac{2}{c_\alpha} \frac{dV^\alpha}{dx_3} + V^\alpha \text{tr}(\mathbf{M}_\alpha) = 0 \quad (9.52)$$

and

$$\frac{1}{c_\alpha} \frac{d\mathbf{M}_\alpha}{dx_3} + \mathbf{M}_\alpha^2 = 0. \quad (9.53)$$

Following exactly the same steps outlined for the fluid case, the solutions of Eqs. (9.52) and (9.53) are then

$$\mathbf{M}_\alpha(x_3) = \mathbf{M}_\alpha(0) [\mathbf{I} + c_\alpha x_3 \mathbf{M}_\alpha(0)]^{-1} \quad (9.54)$$

and

$$\begin{aligned} \frac{V^\alpha(x_3)}{V^\alpha(0)} &= \frac{\sqrt{\det[\mathbf{M}_\alpha^{-1}(0)]}}{\sqrt{\det[\mathbf{M}_\alpha^{-1}(x_3)]}} = \frac{\sqrt{\det[\mathbf{M}_\alpha(x_3)]}}{\sqrt{\det[\mathbf{M}_\alpha(0)]}} \\ &= \frac{1}{\sqrt{\det[\mathbf{I} + c_\alpha x_3 \mathbf{M}_\alpha(0)]}} \end{aligned} \quad (9.55)$$

so that the velocity in the solid for a Gaussian beam of type  $\alpha$  ( $\alpha = p, s$ ) is

$$\begin{aligned} \mathbf{v}^\alpha &= V^\alpha(0) \mathbf{d}^\alpha \frac{\sqrt{\det[\mathbf{M}_\alpha(x_3)]}}{\sqrt{\det[\mathbf{M}_\alpha(0)]}} \\ &\quad \cdot \exp(ik_\alpha x_3) \exp\left(\frac{i\omega}{2} \mathbf{X}^T \mathbf{M}_\alpha(x_3) \mathbf{X}\right) \quad (\alpha = p, s) \end{aligned} \quad (9.56)$$

which shows that apart from the polarization vector the form of a Gaussian beam propagating in a solid is identical to that in a fluid (Eq. (9.33)).

### 9.3 Transmission/Reflection of a Gaussian Beam at an Interface

In the last section, we obtained explicit expressions for a Gaussian beam propagating in either a fluid or a solid. Here, we will obtain the transmission/reflection laws for a Gaussian beam incident on a curved interface between two solids (Fig. 9.8). A fluid-solid interface as found in immersion testing is then merely a special case of these relations. We will consider the case where the Gaussian beam may interact with an interface more than one time so the interface shown in Fig. 9.8 will be used to represent the Gaussian beam on the  $m$ th interface ( $m = 1, 2, \dots$ ).

When the incident Gaussian beam strikes the interface, transmitted and reflected Gaussian beams of various types will be generated. In Fig. 9.8 we show a Gaussian beam incident on a general curved interface  $\Sigma$  between two homogenous, isotropic media (solid or fluid) and only one other Gaussian beam that will be used to represent any one of the transmitted or reflected Gaussian beams generated. We will let the first medium be medium  $m$  and the second medium  $m+1$ . The wave speed of a Gaussian beam type  $\beta$  ( $\beta = p, s$ ) in medium  $m$  and the wave speed of a

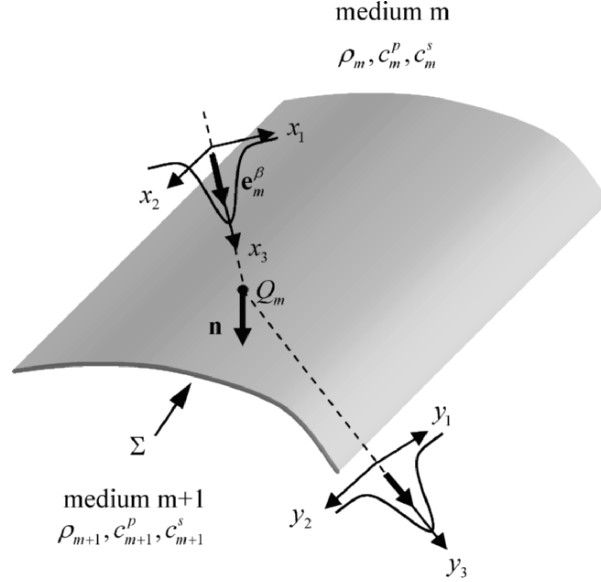


**Fig. 9.8.** A Gaussian beam incident on a curved interface between two elastic media and one of the transmitted or reflected Gaussian beams. The origins of the  $(x_1, x_2, x_3)$  and  $(y_1, y_2, y_3)$  axes are both at the point  $Q_m$  where the central axis of the incident Gaussian beam meets the interface, but these origins are shown displaced for clarity of illustration.

Gaussian beam of type  $\alpha$  ( $\alpha = p, s$ ) in medium  $m+1$  will be given by  $c_m^\beta, c_{m+1}^\alpha$ , respectively, and the corresponding wave numbers by  $k_m^\beta, k_{m+1}^\alpha$ . The velocity amplitude, polarization vector, and complex phase of a Gaussian beam of type  $\beta$  in medium  $m$  and of type  $\alpha$  in medium  $m+1$  will be designated as  $V_m^\beta, \mathbf{d}_m^\beta, \mathbf{M}_m^\beta$  and  $V_{m+1}^\alpha, \mathbf{d}_{m+1}^\alpha, \mathbf{M}_{m+1}^\alpha$ , respectively. The propagation direction of the incident Gaussian beam will be along the  $x_3$ -axis in the  $(x_1, x_2, x_3)$  coordinate system and the propagation of the generated wave will be along the  $y_3$ -axis in the  $(y_1, y_2, y_3)$  coordinates (Fig. 9.8). Unit vectors along both of these propagation directions are given by  $\mathbf{e}_m^\beta, \mathbf{e}_{m+1}^\alpha$ , respectively, as shown. The normal to the interface at the point  $Q_m$  where the central axis of the incident Gaussian beam strikes the interface is the unit vector,  $\mathbf{n}$ . The origins of both the  $(x_1, x_2, x_3)$  and  $(y_1, y_2, y_3)$  axes

will be taken to be at point  $Q_m$ . The origins are shown displaced from  $Q_m$  in Fig. 9.8 for clarity of illustration only.

In relating the Gaussian beams at the interface it will be necessary to perform some coordinate rotations in three dimensions [9.2]. Thus, we need to extend the definition of the 2x2 complex matrices involved to 3x3 matrices in a three-dimensional space. We will denote the 3-D version of matrix  $\mathbf{M}_m^\beta$  as  $\hat{\mathbf{M}}_m^\beta$ , where

$$\hat{\mathbf{M}}_m^\beta = \begin{bmatrix} (\mathbf{M}_m^\beta)_{11} & (\mathbf{M}_m^\beta)_{12} & 0 \\ (\mathbf{M}_m^\beta)_{21} & (\mathbf{M}_m^\beta)_{22} & 0 \\ 0 & 0 & 0 \end{bmatrix} \quad (9.57)$$

with a similar definition for  $\hat{\mathbf{M}}_{m+1}^\alpha$ .

Using the notations just given, we will write the velocity components of the incident Gaussian beam in medium  $m$  as

$$\left(v_m^{\beta;(x)}\right)_j = V_{mj}^{\beta;(x)}(x_3) \exp \left[ i\omega t_0 + ik_m^\beta x_3 + i\frac{\omega}{2} \mathbf{x}^T \hat{\mathbf{M}}_m^{\beta;(x)}(x_3) \mathbf{x} \right], \quad (9.58)$$

where  $V_{mj}^{\beta;(x)}(x_3) = V_m^\beta(x_3) \left(d_m^{\beta;(x)}\right)_j$ . Similarly for a Gaussian beam in medium  $m+1$ :

$$\left(v_{m+1}^{\alpha;(y)}\right)_j = V_{m+1j}^{\alpha;(y)}(y_3) \exp \left[ i\omega t_0 + ik_{m+1}^\alpha y_3 + i\frac{\omega}{2} \mathbf{y}^T \hat{\mathbf{M}}_{m+1}^{\alpha;(y)}(y_3) \mathbf{y} \right] \quad (9.59)$$

where  $V_{m+1j}^{\alpha;(y)}(y_3) = V_{m+1}^\alpha(y_3) \left(d_{m+1}^{\alpha;(y)}\right)_j$ . In both Eq. (9.58) and Eq. (9.59)

$\mathbf{x} = (x_1, x_2, x_3)$  and  $\mathbf{y} = (y_1, y_2, y_3)$  are now full 3-D coordinates. We have placed an  $(x)$  or  $(y)$  in the notation for the vector and matrix terms appearing in Eqs. (9.58) and (9.59) to emphasize that the components involved in those quantities are being calculated in the  $x$ - and  $y$ -coordinates, respectively. This will be useful because it will become necessary to introduce several other coordinate systems when we solve the transmission/reflection problem. The term  $\exp(i\omega t_0)$  appearing in both Eq. (9.58) and (9.59) corresponds to the time delay,  $t_0$ , it has taken for the incident beam to reach point  $Q_m$  on the interface from its starting location (which will be at the transducer face when this Gaussian beam is used to

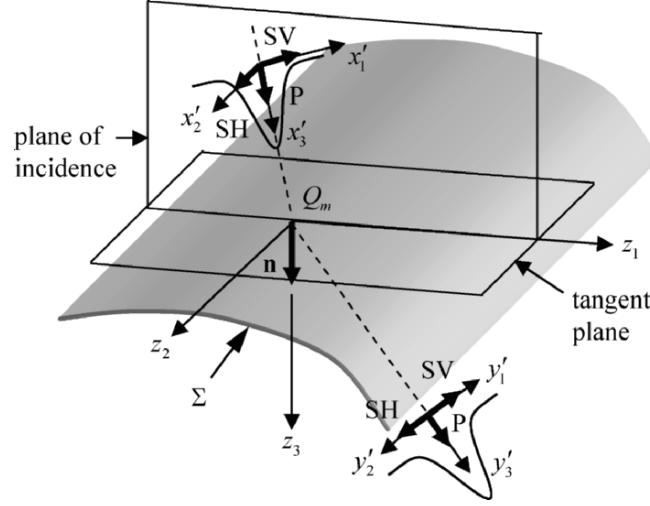


**Fig. 9.9.** Plane of incidence coordinates along the incident and T/R Gaussian beam directions and interface coordinates  $(z_1, z_2, z_3)$ . The origin of all these coordinates is taken at point  $Q_m$  but the incident and T/R axes are shown displaced for clarity of illustration.

represent a transducer wave field). Point  $Q_m$  is at  $x_3 = y_3 = 0$  for both coordinate systems, as mentioned previously.

Most transmission/reflection problems are solved in plane of incidence coordinates. The *plane of incidence* (POI) at interface  $m$  is the plane that contains both the incident wave direction,  $\mathbf{e}_m^\beta$ , and the normal,  $\mathbf{n}$ , to the interface at point  $Q_m$  where the central axis of the incident beam strikes the interface (see Fig. 9.9). The POI coordinates  $(x'_1, x'_2, x'_3)$  for the incident beam are obtained from the  $(x_1, x_2, x_3)$  axes through a 2-D rotation about the  $x_3$ -axis, where  $x_3 = x'_3$  is along the direction of propagation of the incident beam. The  $(x'_1, x'_3)$  axes lie in the POI while the  $x'_2$ -axis is perpendicular to the POI, as shown in Fig. 9.9. Similarly, the POI coordinates  $(y'_1, y'_2, y'_3)$  for the transmitted/reflected beam are obtained from the  $(y_1, y_2, y_3)$  axes through a 2-D rotation about the  $y_3$ -axis, where  $y_3 = y'_3$  is along the direction of propagation of the transmitted/reflected beam. The  $(y'_1, y'_3)$  axes lie in the POI while the  $y'_2$ -axis is perpendicular

to the POI. As for the  $(x_1, x_2, x_3), (y_1, y_2, y_3)$  axes, the origin of both the  $(x'_1, x'_2, x'_3)$  and  $(y'_1, y'_2, y'_3)$  axes will be taken at point  $Q_m$  although those coordinates are shown displaced from  $Q_m$  in Fig. 9.9 for purposes of clarity of illustration. We also define the  $(z_1, z_2, z_3)$  coordinates shown in Fig. 9.9, where  $z_3$  is along the unit normal,  $\mathbf{n}$ ,  $(z_1, z_3)$  lie in the POI, and the  $z_2$ -axis is perpendicular to the POI, as shown. We can express both the incident and transmitted/reflected waves in these  $z$ -coordinates as

$$\left(v_m^{\beta;(z)}\right)_j = V_m^\beta(\mathbf{z}) \left(d_m^{\beta;(z)}\right)_j \exp\left[i\omega t_0 + ik_m^\beta \mathbf{e}_m^\beta \cdot \mathbf{z} + i\phi_m^\beta(\mathbf{z})\right] \quad (9.60)$$

and

$$\left(v_{m+1}^{\alpha;(z)}\right)_j = V_{m+1}^\alpha(\mathbf{z}) \left(d_{m+1}^{\alpha;(z)}\right)_j \exp\left[i\omega t_0 + ik_{m+1}^\alpha \mathbf{e}_{m+1}^\alpha \cdot \mathbf{z} + i\phi_{m+1}^\alpha(\mathbf{z})\right] \quad (9.61)$$

where, to simplify the notation we have lumped all the quadratic phase terms in the  $\phi_m^\beta, \phi_{m+1}^\alpha$  terms.

We require that the velocity components of Eqs. (9.60) and (9.61) satisfy the conditions of velocity and traction matching on the interface  $\Sigma$ . These conditions are

$$\begin{aligned} \sum_\gamma \left(v_m^{\gamma;(z)}(\Sigma)\right)_j &= \sum_\delta \left(v_{m+1}^{\delta;(z)}(\Sigma)\right)_j \\ \sum_\gamma n_i^{(z)} C_{ijkl}^{(m)} \frac{\partial \left(v_m^{\gamma;(z)}(\Sigma)\right)_k}{\partial z_l} &= \sum_\delta n_i^{(z)} C_{ijkl}^{(m+1)} \frac{\partial \left(v_{m+1}^{\delta;(z)}(\Sigma)\right)_k}{\partial z_l}, \end{aligned} \quad (9.62)$$

where  $C_{ijkl}^{(m)}, C_{ijkl}^{(m+1)}$  are the elastic constants for the  $m$ th and  $(m+1)$ th media, respectively. The sums in Eq. (9.62) are taken over all the waves (incident, reflected, or transmitted) of type  $\gamma$  that are present in medium  $m$ , and of type  $\delta$  that are present in medium  $(m+1)$ . We will not satisfy the conditions of Eq. (9.62) exactly over the entire interface  $\Sigma$ . Instead, consistent with the paraxial approximation which treats our Gaussian beams as propagating quasi-plane waves confined to a region near the central beam axis, we will match the “amplitude” parts of Eqs. (9.60) and (9.61) only at point  $Q_m$ , where the amplitudes are just the complex-valued coefficients of the complex exponentials appearing in those equations. The “phase” parts of Eqs. (9.60) and (9.61), however, we will match to second order in the  $z$ -coordinates at point  $Q_m$ , where the phase are the arguments of the

complex exponentials in those equations [Note: we place quotes on the “amplitude” and “phase” terms considered here since they are in fact both complex quantities]. The amplitude matching conditions from Eqs. (9.60), (9.61) and Eq. (9.62) are then

$$\begin{aligned}
 \sum_{\gamma} V_m^{\gamma}(Q_m)(d_m^{\gamma})_j &= \sum_{\delta} V_{m+1}^{\delta}(Q_m)(d_{m+1}^{\delta})_j \\
 \sum_{\gamma} n_i^{(z)} C_{ijkl}^{(m)}(d_m^{\gamma})_k & \\
 \cdot \left[ ik_m^{\gamma} (e_m^{\gamma(z)})_l V_m^{\gamma}(Q_m) + \frac{\partial V_m^{\gamma}}{\partial z_l} \bigg|_{Q_m} + i V_m^{\gamma} \frac{\partial \phi_m^{\gamma}}{\partial z_l} \bigg|_{Q_m} \right] & \quad (9.63) \\
 = \sum_{\delta} n_i C_{ijkl}^{(m+1)}(d_{m+1}^{\delta})_k & \\
 \cdot \left[ ik_{m+1}^{\delta} (e_{m+1}^{\delta})_l V_{m+1}^{\delta}(Q_m) + \frac{\partial V_{m+1}^{\delta}}{\partial z_l} \bigg|_{Q_m} + i V_{m+1}^{\delta} \frac{\partial \phi_{m+1}^{\delta}}{\partial z_l} \bigg|_{Q_m} \right]. &
 \end{aligned}$$

The derivatives of the  $\phi_m^{\gamma}, \phi_{m+1}^{\delta}$  terms appearing in Eq. (9.63) all vanish at  $Q_m$  since these terms are both quadratic functions in the  $z$ -coordinates. Also, at high frequencies the derivatives of the  $V_m^{\gamma}, V_{m+1}^{\delta}$  terms in Eq. (9.63) are much smaller than the terms which only involve the  $V_m^{\gamma}, V_{m+1}^{\delta}$  themselves, since the latter terms are multiplied by the frequency terms  $k_m^{\gamma}, k_{m+1}^{\delta}$ . Thus, Eq. (9.63) reduces to

$$\begin{aligned}
 \sum_{\gamma} V_m^{\gamma}(Q_m)(d_m^{\gamma})_j &= \sum_{\delta} V_{m+1}^{\delta}(Q_m)(d_{m+1}^{\delta})_j \\
 \sum_{\gamma} n_i^{(z)} C_{ijkl}^{(m)}(d_m^{\gamma})_k &\left[ ik_m^{\gamma} (e_m^{\gamma(z)})_l V_m^{\gamma}(Q_m) \right] \\
 = \sum_{\delta} n_i C_{ijkl}^{(m+1)}(d_{m+1}^{\delta})_k &\left[ ik_{m+1}^{\delta} (e_{m+1}^{\delta})_l V_{m+1}^{\delta}(Q_m) \right].
 \end{aligned} \quad (9.64)$$

But the conditions of Eq. (9.64) are just the same as if we had applied the boundary conditions of Eq. (9.62) to a set of plane waves given by

$$(v_m^{\gamma(z)})_j = V_m^{\gamma}(d_m^{\gamma(z)})_j \exp[i\omega t_0 + ik_m^{\gamma} \mathbf{e}_m^{\gamma} \cdot \mathbf{z}] \quad (9.65)$$

$$\left( v_{m+1}^{\delta;(z)} \right)_j = V_{m+1}^{\delta} \left( d_{m+1}^{\delta;(z)} \right)_j \exp \left[ i\omega t_0 + ik_{m+1}^{\delta} \mathbf{e}_{m+1}^{\delta} \cdot \mathbf{z} \right] \quad (9.66)$$

at a plane interface that coincides with the tangent plane to the interface  $\Sigma$  at point  $Q_m$ . The solution of Eq. (9.64), therefore, just yields the appropriate plane wave transmission/reflection (T/R) coefficients. Normally these T/R coefficients are found by assuming a P, SV, or SH polarization direction for the incident and transmitted/reflected (T/R) waves in the POI coordinates  $(x'_1, x'_2, x'_3)$ , as shown in Fig. 9.9, and solving for a corresponding transmitted or reflected P, SV, or SH wave component in the POI coordinates  $(y'_1, y'_2, y'_3)$ . However, our incident beam will not necessarily have a polarization that lies in the POI of the  $m$ th interface. Also, all the incident and T/R waves are not coupled to each other. For example, there is no coupling between plane P-waves or SV-waves and an SH-wave. Thus, it is necessary to define a procedure so that if we have an incident beam of specified type  $\beta$  ( $\beta = p, s$ ) and a T/R beam of specified type  $\alpha$  ( $\alpha = p, s$ ) that the velocity components of these incident and T/R waves are related properly to each other. We can do this by defining a T/R matrix that transforms the  $(x'_1, x'_2, x'_3)$ -components of velocity of the incident wave into the correct  $(y'_1, y'_2, y'_3)$ -components of the T/R wave [9.2]. Specifically, consider the case when we have an incident wave of type S and are considering a T/R wave of the S-wave type ( $S \rightarrow S$ ). Then the  $(y'_1, y'_2, y'_3)$  components of the T/R wave,  $V_{m+1j}^{s;(y')} = V_{m+1}^s \left( d_{m+1}^{s;(y')} \right)_j$ , and the  $(x'_1, x'_2, x'_3)$  components of the incident wave,  $V_{mj}^{s;(x')} = V_m^s \left( d_m^{s;(x')} \right)_j$  can be related to each other by

$$V_{m+1i}^{s;(y')} = \left( \tilde{T}_m^{s;s} \right)_{ij} V_{mj}^{s;(x')}, \quad (9.67)$$

where the 3x3 T/R matrix,  $\tilde{T}_m^{s;s}$ , is

$$\tilde{T}_m^{s;s} = \begin{bmatrix} T_m^{sv;sv} & 0 & 0 \\ 0 & T_m^{sh;sh} & 0 \\ 0 & 0 & 0 \end{bmatrix}. \quad (9.68)$$

whose components are the ordinary plane wave T/R coefficients,  $T_m^{\delta;\gamma}$  (based on velocity ratios) for a T/R plane wave of type  $\delta$  due to a plane



wave of type  $\gamma$  at the  $m$ th interface, where the polarization of the incident and T/R waves used to define these coefficients are defined in Fig. 9.9. For example, the polarization of an incident SV-wave is assumed to be in the  $x'_1$  -direction. Note that this 3x3 matrix properly transforms the individual SV- and SH-components of the incident S-wave (i.e. components along the  $x'_1$  and  $x'_2$  -axes, respectively) into corresponding SV- and SH- components of the T/R wave (i.e. components along the  $y'_1$  and  $y'_2$  -axes, respectively) and does not generate any P-wave ( $y'_3$  component) of the T/R wave, as is required since the T/R wave is specified to be an S-wave. In a similar fashion we can define T/R matrices appropriate to the  $(S \rightarrow P), (P \rightarrow S), (P \rightarrow P)$  cases as

$$\tilde{\mathbf{T}}_m^{p;s} = \begin{bmatrix} 0 & 0 & 0 \\ 0 & 0 & 0 \\ T_m^{p;sv} & 0 & 0 \end{bmatrix} \quad (9.69)$$

and

$$\tilde{\mathbf{T}}_m^{s;p} = \begin{bmatrix} 0 & 0 & T_m^{sv;p} \\ 0 & 0 & 0 \\ 0 & 0 & 0 \end{bmatrix} \quad (9.70)$$

and

$$\tilde{\mathbf{T}}_m^{p;p} = \begin{bmatrix} 0 & 0 & 0 \\ 0 & 0 & 0 \\ 0 & 0 & T_m^{p;p} \end{bmatrix}. \quad (9.71)$$

With these definitions, then for the general case we can write simply

$$V_{m+1i}^{\alpha;(y')} = \left( \tilde{T}_m^{\alpha;\beta} \right)_{ij} V_{mj}^{\beta;(x')} \quad (9.72)$$

We now need to transform this relationship back into our original  $(x_1, x_2, x_3)$  and  $(y_1, y_2, y_3)$  coordinates. Let  $(\mathbf{u}_1, \mathbf{u}_2, \mathbf{u}_3)$  be unit vectors along the  $(x_1, x_2, x_3)$  axes, respectively, and similarly let  $(\mathbf{u}'_1, \mathbf{u}'_2, \mathbf{u}'_3)$  be unit vectors along the  $(x'_1, x'_2, x'_3)$  POI axes. Also, let  $(\mathbf{v}_1, \mathbf{v}_2, \mathbf{v}_3)$  be unit vectors along the  $(y_1, y_2, y_3)$  axes, and  $(\mathbf{v}'_1, \mathbf{v}'_2, \mathbf{v}'_3)$  be unit vectors along the  $(y'_1, y'_2, y'_3)$  POI axes. We can choose the  $(y_1, y_2)$  axes to have any

orientation we wish about the T/R wave direction,  $y_3$ , but a particularly convenient choice is to make the orientation  $(y_1, y_2)$  axes relative to the  $(y'_1, y'_2)$  axes the same as the orientation of the  $(x_1, x_2)$  axes relative to the  $(x'_1, x'_2)$  axes (this is called the “standard” choice in [9.2]). With this choice, when the material is the same on both sides of the interface Eq. (9.72) will simply leave the  $(y_1, y_2, y_3)$  components of the velocity unchanged from the original  $(x_1, x_2, x_3)$  components. Based on this choice, we can define a 3-D rotation matrix,  $\hat{\mathbf{G}}^R$ , with components  $\hat{G}_{np}^R = (\mathbf{u}'_n \cdot \mathbf{u}_p) = (\mathbf{v}'_n \cdot \mathbf{v}_p)$  where

$$\begin{aligned} \hat{\mathbf{G}}^R &= \begin{bmatrix} \mathbf{u}'_1 \cdot \mathbf{u}_1 & \mathbf{u}'_1 \cdot \mathbf{u}_2 & 0 \\ \mathbf{u}'_2 \cdot \mathbf{u}_1 & \mathbf{u}'_2 \cdot \mathbf{u}_2 & 0 \\ 0 & 0 & 1 \end{bmatrix} = \begin{bmatrix} \mathbf{v}'_1 \cdot \mathbf{v}_1 & \mathbf{v}'_1 \cdot \mathbf{v}_2 & 0 \\ \mathbf{v}'_2 \cdot \mathbf{v}_1 & \mathbf{v}'_2 \cdot \mathbf{v}_2 & 0 \\ 0 & 0 & 1 \end{bmatrix} \\ &= \begin{bmatrix} \cos \lambda & \sin \lambda & 0 \\ -\sin \lambda & \cos \lambda & 0 \\ 0 & 0 & 1 \end{bmatrix} \end{aligned} \quad (9.73)$$

and we have

$$\begin{aligned} V_{mj}^{\beta;(x')} &= \hat{G}_{jp}^R V_{mp}^{\beta;(x)} \\ V_{m+1i}^{\alpha;(y')} &= \hat{G}_{ir}^R V_{m+1r}^{\alpha;(y)} \end{aligned} \quad (9.74)$$

which, when placed into Eq. (9.72) gives

$$\hat{G}_{ir}^R V_{m+1r}^{\alpha;(y)} = \left( \tilde{T}_m^{\alpha;\beta} \right)_{ij} \hat{G}_{jp}^R V_{mp}^{\beta;(x)}. \quad (9.75)$$

If we pre-multiply Eq. (9.75) by  $\hat{G}_{ik}^R$  and use the fact that  $\hat{G}_{ik}^R \hat{G}_{ir}^R = \delta_{kr}$ , we find

$$V_{m+1k}^{\alpha;(y)} = \hat{G}_{ik}^R \left( \tilde{T}_m^{\alpha;\beta} \right)_{ij} \hat{G}_{jp}^R V_{mp}^{\beta;(x)} \quad (9.76)$$

or, equivalently

$$V_{m+1}^{\alpha}(\mathcal{Q}_m) \left( d_{m+1}^{\alpha;(y)} \right)_k = \left( T_m^{\alpha;\beta} \right)_{kp} V_m^{\beta}(\mathcal{Q}_m) \left( d_m^{\beta;(x)} \right)_p, \quad (9.77)$$

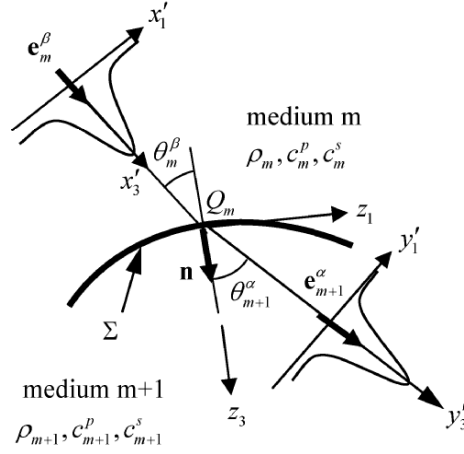


**Fig. 9.10.** The angles that an incident and transmitted Gaussian beam make at the interface in the POI coordinates.

where

$$\left( T_m^{\alpha;\beta} \right)_{kp} = \hat{G}_{jk}^R \left( \tilde{T}_m^{\alpha;\beta} \right)_{ij} \hat{G}_{jp}^R \quad (9.78)$$

Equation (9.77) gives the relationship needed to obtain the amplitude of the T/R Gaussian beam from the incident beam. In many NDE testing situations the POI for all the interfaces may be aligned and we can always assume that the  $(x_1, x_2, x_3)$  and  $(y_1, y_2, y_3)$  coordinates are the same as the POI coordinates. In that case the rotation matrix,  $\hat{\mathbf{G}}^R$ , is not needed and the wave types  $\alpha$  and  $\beta$  range over  $(p, sv)$  only so we write

$$V_{m+1}^\alpha(Q_m) = T_m^{\alpha;\beta} V_m^\beta(Q_m) \quad (9.79)$$

without using a 3x3 T/R matrix. The polarization directions for the incident and T/R waves are then just the directions shown in Fig. 9.9. Figure 9.10 shows explicitly the acute angle  $\theta_m^\beta$  that the direction of propagation an incident wave of type  $\beta$  makes with respect to the interface normal ( $z_3$ -axis) and the acute angle  $\theta_{m+1}^\alpha$  for a transmitted wave of type  $\alpha$ . These angles will be needed as we now discuss the phase matching of the Gaussian beams at the interface.

The total phase of the complex exponential term in Eq. (9.58) for the incident wave in medium  $m$  is

$$\Phi_m^\beta = i\omega t_0 + ik_m^\beta x_3 + i\frac{\omega}{2} \mathbf{x}^T \hat{\mathbf{M}}_m^{\beta(x)}(x_3) \mathbf{x} \quad (9.80)$$

Similarly the total phase for a transmitted wave in medium  $m+1$  from Eq. (9.59) is

$$\Phi_{m+1}^\alpha = i\omega t_0 + ik_{m+1}^\alpha y_3 + i\frac{\omega}{2} \mathbf{y}^T \hat{\mathbf{M}}_{m+1}^{\alpha(y)}(y_3) \mathbf{y}. \quad (9.81)$$

Here, we will match these phases at the interface,  $\Sigma$ , in the  $(z_1, z_2, z_3)$  coordinates in a neighborhood of the point  $Q_m$ . Consider first Eq. (9.80) for the incident wave. To transform from the  $(x_1, x_2, x_3)$  coordinates to the  $(z_1, z_2, z_3)$  coordinates, we first use the rotation matrix previously defined to transform from  $(x_1, x_2, x_3)$  to  $(x'_1, x'_2, x'_3)$  POI coordinates (by rotating about the  $x_3$ -axis). We then transform from the  $(x'_1, x'_2, x'_3)$  coordinates to the  $(z_1, z_2, z_3)$  coordinates through a rotation about an angle  $\theta_m^\beta$  about the  $x'_2$ -axis, i.e. we let

$$\begin{aligned} x_i &= \hat{G}_{ki}^R x'_k \\ x'_k &= \hat{G}_{jk}^Z z_j, \end{aligned} \quad (9.82)$$

where  $\mathbf{G}^R$  has been given previously (Eq. (9.73)) and  $\hat{\mathbf{G}}^Z$  is the rotation matrix

$$\hat{\mathbf{G}}^Z = \begin{bmatrix} \cos \theta_m^\alpha & 0 & \sin \theta_m^\alpha \\ 0 & 1 & 0 \\ -\sin \theta_m^\alpha & 0 & \cos \theta_m^\alpha \end{bmatrix}. \quad (9.83)$$

If we combine the two rotation matrices into a single matrix,  $\hat{\mathbf{G}}^C$ , where

$$\hat{G}_{ji}^C = \hat{G}_{ki}^R \hat{G}_{jk}^Z \quad (9.84)$$

then the total phase of the incident wave in the  $(z_1, z_2, z_3)$  coordinates can be written as

$$\begin{aligned}\Phi_m^\beta &= i\omega t_0 + ik_m^\beta (z_1 \sin \theta_m^\beta + z_3 \cos \theta_m^\beta) \\ &+ i\frac{\omega}{2} \left( \hat{\mathbf{M}}_m^{\beta;(x)}(\mathcal{Q}_m) \right)_{ij} \hat{G}_{pi}^C \hat{G}_{rj}^C z_p z_r.\end{aligned}\quad (9.85)$$

In the neighborhood of point  $\mathcal{Q}_m$  for a curved interface we have to second order

$$z_3 = \frac{1}{2} h_{IJ}(\mathcal{Q}_m) z_I z_J, \quad (9.86)$$

where the summation over capital subscripts such as the I and J in Eq. (9.86) is taken over the values (1,2) only. This is a convention we will also follow in subsequent expressions. The components of the 2x2 matrix  $h_{IJ}$  in Eq. (9.86) are the curvatures of the interface at  $\mathcal{Q}_m$  as measured in the  $z$ -coordinates, with  $z_3$  along the interface normal and  $z_1$  in the plane of incidence, as shown in Figs. 9.9 and 9.10.

We now place Eq. (9.86) into Eq. (9.85), keeping only the terms which are at most quadratic in the  $(z_1, z_2)$  coordinates and use the fact that

$$\left( \hat{\mathbf{M}}_m^{\beta;(x)}(\mathcal{Q}_m) \right)_{I3} = \left( \hat{\mathbf{M}}_m^{\beta;(x)}(\mathcal{Q}_m) \right)_{3I} = \left( \hat{\mathbf{M}}_m^{\beta;(x)}(\mathcal{Q}_m) \right)_{33} = 0. \quad (I=1,2) \quad (9.87)$$

Then Eq. (9.85) becomes

$$\begin{aligned}\Phi_m^\beta &= i\omega t_0 + ik_m^\beta z_1 \sin \theta_m^\beta \\ &+ i\frac{\omega}{2} \left( \left( \hat{\mathbf{M}}_m^{\beta;(x)}(\mathcal{Q}_m) \right)_{IJ} G_{PI}^C G_{RJ}^C + h_{PR}(\mathcal{Q}_m) \frac{\cos \theta_m^\beta}{c_m^\beta} \right) z_P z_R.\end{aligned}\quad (9.88)$$

In Eq. (9.88) all the capital subscripts take on the values (1,2) only so the  $\mathbf{M}_m^\alpha$  matrix in that equation is the 2x2 sub-matrix of  $\hat{\mathbf{M}}_m^\alpha$  and similarly the rotation matrices in Eq. (9.88) only involve 2x2 sub-matrices of  $\hat{\mathbf{G}}^C$ , given by

$$\mathbf{G}^C = \mathbf{G}^Z \mathbf{G}^R = \begin{bmatrix} \cos \theta_m^\beta & 0 \\ 0 & 1 \end{bmatrix} \begin{bmatrix} \cos \lambda & \sin \lambda \\ -\sin \lambda & \cos \lambda \end{bmatrix}. \quad (9.89)$$

Equation (9.88) is an (approximate) expression for the total phase of a Gaussian beam for the incident beam in medium  $m$ . For a transmitted wave in medium  $m+1$  in an entirely similar fashion one obtains:

$$\Phi_{m+1}^\alpha = i\omega t_0 + ik_{m+1}^\alpha z_1 \sin \theta_{m+1}^\alpha + i\frac{\omega}{2} \left( \left( \mathbf{M}_{m+1}^{\alpha;(y)}(Q_m) \right)_{IJ} \tilde{G}_{PI}^C \tilde{G}_{RJ}^C + h_{PR}(Q_m) \frac{\cos \theta_{m+1}^\alpha}{c_{m+1}^\alpha} \right) z_P z_R, \quad (9.90)$$

where

$$\tilde{\mathbf{G}}^C = \tilde{\mathbf{G}}^Z \mathbf{G}^R = \begin{bmatrix} \cos \theta_{m+1}^\alpha & 0 \\ 0 & 1 \end{bmatrix} \begin{bmatrix} \cos \lambda & \sin \lambda \\ -\sin \lambda & \cos \lambda \end{bmatrix}. \quad (9.91)$$

Equating the total phases in Eq. (9.88) and Eq. (9.90) the terms involving  $t_0$  cancel. We find from the term that is linear in  $z_1$ :

$$\frac{\sin \theta_{m+1}^\alpha}{c_{m+1}^\alpha} = \frac{\sin \theta_m^\beta}{c_m^\beta}, \quad (9.92)$$

which is a statement of generalized Snell's law. From equality of the quadratic terms it follows that

$$\begin{aligned} & \left( \mathbf{M}_{m+1}^{\alpha;(y)}(Q_m) \right)_{IJ} \tilde{G}_{PI}^C \tilde{G}_{RJ}^C + h_{PR}(Q_m) \frac{\cos \theta_{m+1}^\alpha}{c_{m+1}^\alpha} \\ &= \left( \mathbf{M}_m^{\beta;(x)}(Q_m) \right)_{IJ} G_{PI}^C G_{RJ}^C + h_{PR}(Q_m) \frac{\cos \theta_m^\beta}{c_m^\beta} \end{aligned} \quad (9.93)$$

or, equivalently

$$\begin{aligned} \left( \mathbf{M}_{m+1}^{\alpha;(y)}(Q_m) \right)_{VU} &= \left[ \tilde{G}_{VP}^C \right]^{-1} \left[ \tilde{G}_{UR}^C \right]^{-1} \left( \mathbf{M}_m^{\beta;(x)}(Q_m) \right)_{IJ} G_{PI}^C G_{RJ}^C \\ &+ \left[ \tilde{G}_{VP}^C \right]^{-1} \left[ \tilde{G}_{UR}^C \right]^{-1} h_{PR}(Q_m) \left( \frac{\cos \theta_m^\beta}{c_m^\beta} - \frac{\cos \theta_{m+1}^\alpha}{c_{m+1}^\alpha} \right). \end{aligned} \quad (9.94)$$

Equation (9.94) gives the transformation law across the interface for the  $\mathbf{M}$  matrix of a transmitted beam of type  $\alpha$  in medium  $m+1$  due to an incident wave of type  $\beta$  in medium  $m$ . The same equation also applies to a reflected beam of type  $\alpha$  traveling in medium  $m$  if everywhere in Eq. (9.94) we simply replace  $c_{m+1}^\alpha$  by  $c_m^\alpha$  and  $\cos \theta_{m+1}^\alpha$  by  $-\cos \theta_m^\alpha$  where  $\theta_m^\alpha$  is then the acute angle between the negative  $z_3$ -axis and the propagation direction of the reflected beam. This process corresponds to making the replacement  $\theta_{m+1}^\alpha \rightarrow \pi - \theta_m^\alpha$  and then interpreting  $\theta_m^\alpha$  as the

acute angle that the direction of propagation the reflected wave makes with the negative  $z_3$  axis.

Taking the real part of both sides of Eq. (9.94) gives the transformation of the wave front curvature of the Gaussian beam across the interface. That expression is the same as that found for wave front curvature changes from geometrical ray theory [9.2]. The imaginary parts of Eq. (9.94) relate the beam widths of the Gaussians on either side of the interface in terms of their projections on the interface [9.2]. To see this transformation law in a simple setting, consider a circularly symmetric Gaussian beam given by Eqs. (9.34) and (9.37) incident on a planar interface ( $h_{PR} = 0$ ) where the  $(x_1, x_2, x_3)$  axes are aligned with the POI so that the rotation angle  $\lambda = 0$ . Then we find

$$\mathbf{M}_{m+1}^{\alpha;(y)}(Q_m) = \begin{bmatrix} \frac{\cos^2 \theta_m^\beta}{c_m^\beta \cos^2 \theta_{m+1}^\alpha} \left( \frac{1}{R(Q_m)} + \frac{i c_m^\beta}{\pi f w^2(Q_m)} \right) & 0 \\ 0 & \frac{1}{c_m^\beta} \left( \frac{1}{R(Q_m)} + \frac{i c_m^\beta}{\pi f w^2(Q_m)} \right) \end{bmatrix}, \quad (9.95)$$

where  $f$  is the frequency. Equation (9.95) shows that the circularly symmetric incident beam is transformed into a T/R beam of elliptical cross section with wave front curvatures  $(R_1, R_2)$  and beam widths  $(w_1, w_2)$ , both along the  $(y_1, y_2)$  directions, respectively, where

$$\mathbf{M}_{m+1}^{\alpha;(y)}(Q_m) = \begin{bmatrix} \frac{1}{c_{m+1}^\alpha} \left( \frac{1}{R_1(Q_m)} + \frac{i c_{m+1}^\alpha}{\pi f w_1^2(Q_m)} \right) & 0 \\ 0 & \frac{1}{c_{m+1}^\alpha} \left( \frac{1}{R_2(Q_m)} + \frac{i c_{m+1}^\alpha}{\pi f w_2^2(Q_m)} \right) \end{bmatrix}. \quad (9.96)$$

Equating Eqs. (9.95) and (9.96) gives the transformation laws for the wave front curvatures and beam widths as:

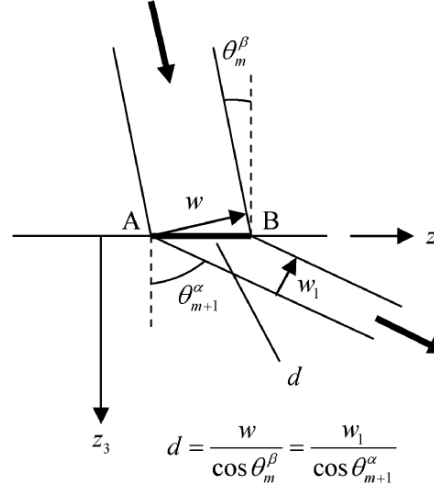


**Fig. 9.11.** The transmission of an incident circular Gaussian beam at an interface showing the change of beam width in the POI, where the incident and transmitted beams both have a common width,  $d$ , between points A and B on the interface. The beam width in the direction normal to the POI is unchanged. This leads to a transmitted beam of elliptical cross-section.

$$\begin{aligned}
 w_1(Q_m) &= \left| \frac{\cos \theta_{m+1}^\alpha}{\cos \theta_m^\beta} \right| w(Q_m) \\
 w_2(Q_m) &= w(Q_m) \\
 R_1(Q_m) &= \frac{c_m^\beta}{c_{m+1}^\alpha} \frac{\cos^2 \theta_{m+1}^\alpha}{\cos^2 \theta_m^\beta} R(Q_m) \\
 R_2(Q_m) &= \frac{c_m^\beta}{c_{m+1}^\alpha} R(Q_m).
 \end{aligned} \tag{9.97}$$

Thus, in the plane of incidence at a planar interface, Eq. (9.97) shows that the incident beam width  $w$  is changed to  $w_1$  where the widths of incident and transmitted beams in the POI have the same projection on the interface, as shown in Fig. 9.11. In contrast  $w_2 = w$  so the beam width in the direction normal to the POI is unchanged. The wave front curvatures are also changed but those changes depend on both the angles present and the wave speeds of the two materials. In Appendix F the special case when a circular Gaussian beam is normal to a planar interface was considered.



Setting  $\theta_{m+1}^\alpha = \theta_m^\beta = 0$  in Eq. (9.97) then yields the same results found there (see Eqs. (F.44) and (F.46)).

Both the propagation and transmission laws do not affect the symmetry of the complex  $\mathbf{M}$  matrix, as can be seen from Eq. (9.28) and Eq. (9.93). Thus, an  $\mathbf{M}$  matrix that starts out symmetric remains symmetric after propagation in multiple media and after interactions with multiple interfaces. Like the propagation law, the interface transformation law of Eq. (9.94) also does not affect the sign on the eigenvalues of the imaginary part of the  $\mathbf{M}$  matrix so that a localized Gaussian remains a localized Gaussian after interactions with the interface. For the simple case just discussed this is obvious since Eq. (9.97) shows that the beam widths on transmission or reflection remain positive, finite values. For the more general case, take the imaginary part of both sides of Eq. (9.93) and let  $\mathbf{M}_{m+1}^I = \text{Im}\{\mathbf{M}_{m+1}^{\alpha;(y)}(Q_m)\}$ ,  $\mathbf{M}_m^I = \text{Im}\{\mathbf{M}_m^{\beta;(x)}(Q_m)\}$ . Then we find

$$\begin{aligned}\mathbf{M}_{m+1}^I &= \left[ (\mathbf{G}^R)^T (\tilde{\mathbf{G}}^Z)^{-1} \mathbf{G}^Z \mathbf{G}^R \right] \mathbf{M}_m^I \left[ (\mathbf{G}^R)^T (\tilde{\mathbf{G}}^Z)^{-1} \mathbf{G}^Z \mathbf{G}^R \right]^T \\ &= \mathbf{P}^T \mathbf{M}_m^I \mathbf{P},\end{aligned}\quad (9.98)$$

where  $(\mathbf{G}^Z)^T = (\mathbf{G}^Z)$ ,  $(\tilde{\mathbf{G}}^Z)^T = (\tilde{\mathbf{G}}^Z)$  and  $(\tilde{\mathbf{G}}^Z)^{-1} \mathbf{G}^Z = \mathbf{G}^Z (\tilde{\mathbf{G}}^Z)^{-1}$ .

The matrix  $\mathbf{P} = \mathbf{P}^T = (\mathbf{G}^R)^T (\tilde{\mathbf{G}}^Z)^{-1} \mathbf{G}^Z \mathbf{G}^R$  is non-singular since for any angles  $\theta_m^\beta, \theta_{m+1}^\alpha \neq \pi/2$  we have

$$\begin{aligned}\det[\mathbf{P}] &= \det[(\mathbf{G}^R)^T] \det[(\tilde{\mathbf{G}}^Z)^{-1}] \det[\mathbf{G}^Z] \det[\mathbf{G}^R] \\ &= (1) \left( \frac{1}{\cos \theta_{m+1}^\alpha} \right) (\cos \theta_m^\beta) (1) \neq 0.\end{aligned}\quad (9.99)$$

Because the eigenvalues of  $\mathbf{M}_m^I$  are positive, the matrix  $\mathbf{M}_m^I$  is positive definite, i.e.  $\mathbf{x}^T \mathbf{M}_m^I \mathbf{x} > 0$  for all real non-trivial vectors,  $\mathbf{x}$ . Then if we let  $\mathbf{x} = \mathbf{P} \mathbf{y}$  where  $\mathbf{y} \neq 0$  (which implies that  $\mathbf{P}$  is non-singular) we have  $\mathbf{y}^T \mathbf{P}^T \mathbf{M}_m^I \mathbf{P} \mathbf{y} > 0$  so it follows from Eq. (9.98) that  $\mathbf{M}_{m+1}^I$  is also positive definite and its eigenvalues are positive.

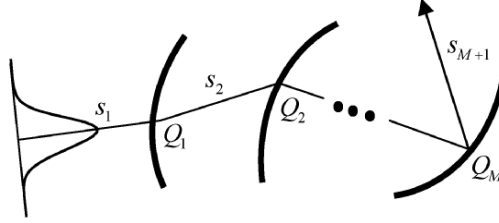


**Fig. 9.12.** The transmission/reflection of a Gaussian beam through multiple media with curved interfaces.

### 9.4 Gaussian Beams and ABCD Matrices

Since a Gaussian beam that starts out localized remains localized during propagation and after interaction with general curved surfaces, the beam is always well behaved, unlike plane waves or spherical waves that can lead to caustics or singularities. Furthermore, we can easily combine the propagation and interface transformation laws to obtain the form of the Gaussian beam after multiple interactions with curved surfaces or interfaces. To see this, consider now the general case where a Gaussian beam travels through or is reflected from  $M$  interfaces, as shown in Fig. 9.12. If we apply the propagation and transmission/reflection laws just derived to each medium and interface, the velocity of the Gaussian beam of type  $\alpha$  in medium  $M+1$  is then given by

$$\begin{aligned} \mathbf{v}_{M+1}^{\alpha(y)} &= \frac{\sqrt{\det[\mathbf{M}_{M+1}^{\alpha}(s_{M+1})]}}{\sqrt{\det[\mathbf{M}_{M+1}^{\alpha}(0)]}} \\ &\cdot \left[ \prod_{m=M}^1 \mathbf{T}_m^{\gamma_{m+1}, \gamma_m} \frac{\sqrt{\det[\mathbf{M}_m^{\gamma_m}(s_m)]}}{\sqrt{\det[\mathbf{M}_m^{\gamma_m}(0)]}} \right] \\ &\cdot V_1^{\gamma_1}(0) \mathbf{d}_1^{\gamma_1} \exp \left[ i\omega \sum_{m=1}^{M+1} \frac{s_m}{c_m^{\gamma_m}} + i \frac{\omega}{2} \mathbf{y}^T \hat{\mathbf{M}}_{M+1}^{\alpha}(s_{M+1}) \mathbf{y} \right] \end{aligned} \quad (9.100a)$$

or, equivalently

$$\begin{aligned}
\mathbf{v}_{M+1}^{\alpha;(y)} = & \frac{1}{\sqrt{\det[\mathbf{I} + s_{M+1} \mathbf{c}_{M+1}^\alpha \mathbf{M}_{M+1}^\alpha(0)]}} \\
& \cdot \left[ \prod_{m=M}^1 \frac{\mathbf{T}_m^{\gamma_{m+1};\gamma_m}}{\sqrt{\det[\mathbf{I} + s_m \mathbf{c}_m^{\gamma_m} \mathbf{M}_m^{\gamma_m}(0)]}} \right] \\
& \cdot V_1^{\gamma_1}(0) \mathbf{d}_1^{\gamma_1} \exp \left[ i\omega \sum_{m=1}^{M+1} \frac{s_m}{c_m^{\gamma_m}} + i \frac{\omega}{2} \mathbf{y}^T \hat{\mathbf{M}}_{M+1}^\alpha(s_{M+1}) \mathbf{y} \right],
\end{aligned} \tag{9.100b}$$

where  $s_m$  is the distance the beam has traveled in medium  $m$  along its central axis and  $\gamma_m$  is the mode of the beam propagating in medium  $m$  and  $\gamma_{m+1}$  is the transmitted or reflected mode in medium  $m+1$  after interaction with the  $m$ -th interface. The matrix  $\mathbf{T}_m^{\gamma_{m+1};\gamma_m}$  is given from Eq. (9.78) by

$$\mathbf{T}_m^{\gamma_{m+1};\gamma_m} = (\hat{\mathbf{G}}^R)^T \tilde{\mathbf{T}}_m^{\gamma_{m+1};\gamma_m} \hat{\mathbf{G}}^R. \tag{9.101}$$

As Eqs. (9.100a) and (9.100b) indicate the product of matrices is in the order

$$\mathbf{T}_M^{\gamma_{M+1};\gamma_M} \mathbf{T}_{M-1}^{\gamma_M;\gamma_{M-1}} \dots \mathbf{T}_1^{\gamma_2;\gamma_1}. \tag{9.102}$$

Note that at the  $m$ -th interface  $\mathbf{M}_m^{\gamma_m}(s_m) = \mathbf{M}_m^{\gamma_m}(Q_m)$  if  $s_m$  is the distance the Gaussian beam has traveled in medium  $m$  to the  $m$ -th interface and  $\mathbf{M}_{m+1}^{\gamma_{m+1}}(0) = \mathbf{M}_{m+1}^{\gamma_{m+1}}(Q_m)$  since point  $Q_m$  is at the starting point for the Gaussian beam in medium  $m+1$ . Thus, we can use either of these notations interchangeably.

Both Eq. (9.100a) and Eq. (9.100b) are remarkably compact in form. The calculation of individual terms in those equations can be done in a highly modular and efficient way by the introduction of **A**, **B**, **C**, **D** matrices which are analogous to the scalar A, B, C, D terms discussed in Appendix F and commonly used in optics [9.7]. These matrices arise from the fact that both the propagation and transmission laws for  $\mathbf{M}_m^{\gamma_m}$  can be written in a common form. First consider the propagation law (Eq. (9.27)). That law can be written as:

$$\mathbf{M}_m^{\gamma_m}(s_m) = [\mathbf{D}_m^d \mathbf{M}_m^{\gamma_m}(0) + \mathbf{C}_m^d] [\mathbf{A}_m^d + \mathbf{B}_m^d \mathbf{M}_m^{\gamma_m}(0)]^{-1}, \tag{9.103}$$

where  $\mathbf{A}_m^d, \mathbf{B}_m^d, \mathbf{C}_m^d, \mathbf{D}_m^d$  will denote the  $\mathbf{A}, \mathbf{B}, \mathbf{C}, \mathbf{D}$  matrices that characterize propagation (displacement) of the beam in medium  $m$ . These matrices also depend on the wave type,  $\gamma_m$ , being considered in the  $m$ -th medium but for economy of notation we will not show that dependency explicitly. Comparing Eqs. (9.27) and (9.103) we find

$$\mathbf{A}_m^d = \mathbf{D}_m^d = \mathbf{I}, \quad \mathbf{B}_m^d = c_m^{\gamma_m} S_m \mathbf{I}, \quad \mathbf{C}_m^d = \mathbf{O}, \quad (9.104)$$

where  $\mathbf{O}$  is the zero matrix. Now, consider the transmission law (Eq. (9.94)). First we rewrite that equation as

$$\begin{aligned} \mathbf{M}_{m+1}^{\gamma_{m+1}}(Q_m) = & \left\{ \left[ \tilde{\mathbf{G}}^C \right]^{-1} \mathbf{G}^C \mathbf{M}_m^{\gamma_m}(Q_m) \right. \\ & \left. + \left[ \tilde{\mathbf{G}}^C \right]^{-1} \mathbf{h}(Q_m) \left( \frac{\cos \theta_m^{\gamma_m}}{c_m^{\gamma_m}} - \frac{\cos \theta_{m+1}^{\gamma_{m+1}}}{c_{m+1}^{\gamma_{m+1}}} \right) \left[ \left[ \mathbf{G}^C \right]^T \right]^{-1} \right\} \left[ \left[ \tilde{\mathbf{G}}^C \right]^{-1} \mathbf{G}^C \right]^T \end{aligned} \quad (9.105)$$

which is also of the form

$$\mathbf{M}_{m+1}^{\gamma_{m+1}}(Q_m) = \left[ \mathbf{D}_m^t \mathbf{M}_m^{\gamma_m}(Q_m) + \mathbf{C}_m^t \right] \left[ \mathbf{A}_m^t + \mathbf{B}_m^t \mathbf{M}_m^{\gamma_m}(Q_m) \right]^{-1}, \quad (9.106)$$

where the transmission matrices  $\mathbf{A}_m^t, \mathbf{C}_m^t$  are

$$\begin{aligned} \mathbf{A}_m^t &= \left[ \tilde{\mathbf{G}}^C \right]^T \left[ \left[ \mathbf{G}^C \right]^T \right]^{-1} \\ &= \begin{bmatrix} \cos \lambda & -\sin \lambda \\ \sin \lambda & \cos \lambda \end{bmatrix} \begin{bmatrix} \frac{\cos \theta_{m+1}^{\gamma_{m+1}}}{\cos \theta_m^{\gamma_m}} & 0 \\ 0 & 1 \end{bmatrix} \begin{bmatrix} \cos \lambda & \sin \lambda \\ -\sin \lambda & \cos \lambda \end{bmatrix}, \end{aligned} \quad (9.107a)$$

and

$$\begin{aligned} \mathbf{C}_m^t &= \left( \frac{\cos \theta_m^{\gamma_m}}{c_m^{\gamma_m}} - \frac{\cos \theta_{m+1}^{\gamma_{m+1}}}{c_{m+1}^{\gamma_{m+1}}} \right) \left[ \tilde{\mathbf{G}}^C \right]^{-1} \mathbf{h}(Q_m) \left[ \left[ \mathbf{G}^C \right]^T \right]^{-1} \\ &= \left( \frac{\cos \theta_m^{\gamma_m}}{c_m^{\gamma_m}} - \frac{\cos \theta_{m+1}^{\gamma_{m+1}}}{c_{m+1}^{\gamma_{m+1}}} \right) \begin{bmatrix} \cos \lambda & -\sin \lambda \\ \sin \lambda & \cos \lambda \end{bmatrix} \\ &\quad \cdot \begin{bmatrix} \frac{h_{11}}{\cos \theta_{m+1}^{\gamma_{m+1}} \cos \theta_m^{\gamma_m}} & \frac{h_{12}}{\cos \theta_{m+1}^{\gamma_{m+1}}} \\ \frac{h_{21}}{\cos \theta_m^{\gamma_m}} & h_{22} \end{bmatrix} \begin{bmatrix} \cos \lambda & \sin \lambda \\ -\sin \lambda & \cos \lambda \end{bmatrix} \end{aligned} \quad (9.107b)$$

and the  $\mathbf{B}_m^t$ ,  $\mathbf{D}_m^t$  matrices are

$$\mathbf{B}_m^t = \mathbf{O} \quad (9.107c)$$

$$\mathbf{D}_m^t = [\tilde{\mathbf{G}}^C]^{-1} \mathbf{G}^C = \begin{bmatrix} \cos \lambda & -\sin \lambda \\ \sin \lambda & \cos \lambda \end{bmatrix} \cdot \begin{bmatrix} \frac{\cos \theta_m^{\gamma_m}}{\cos \theta_{m+1}^{\gamma_{m+1}}} & 0 \\ 0 & 1 \end{bmatrix} \begin{bmatrix} \cos \lambda & \sin \lambda \\ -\sin \lambda & \cos \lambda \end{bmatrix}. \quad (9.107d)$$

The  $t$  superscript indicates these matrices are transmission matrices. They are also functions of the wave types  $\gamma_{m+1}, \gamma_m$  but again for notational simplicity we will not show that dependency explicitly. Note that the equivalent  $\mathbf{A}$ ,  $\mathbf{B}$ ,  $\mathbf{C}$ ,  $\mathbf{D}$  matrices for a reflected wave at the  $m$ -th interface can be obtained by replacing  $c_{m+1}^{\gamma_{m+1}}$  by  $c_m^{\gamma_{m+1}}$  and  $\cos \theta_{m+1}^{\gamma_{m+1}}$  by  $-\cos \theta_m^{\gamma_{m+1}}$  in all the matrices of Eqs. (9.107a - d).

We have shown that both the propagation and transmission laws for a Gaussian beam can be represented in identical forms in terms  $\mathbf{A}$ ,  $\mathbf{B}$ ,  $\mathbf{C}$ , and  $\mathbf{D}$  matrices. This representation is important since if we propagate a Gaussian beam in medium  $m$  from  $s_m = 0$  (where the  $\mathbf{M}$  matrix is  $\mathbf{M}_m^{\gamma_m}(0)$ ) over a distance  $s_m$  to interface  $m$  (where the  $\mathbf{M}$  matrix is  $\mathbf{M}_m^{\gamma_m}(Q_m)$ ) and then transmit that beam across interface  $m$  to obtain  $\mathbf{M}_{m+1}^{\gamma_{m+1}}(Q_m)$ , the relationship between the  $\mathbf{M}_{m+1}^{\gamma_{m+1}}(Q_m)$  and  $\mathbf{M}_m^{\gamma_m}(0)$  after both types of interactions can also be written as

$$\mathbf{M}_{m+1}^{\gamma_{m+1}}(Q_m) = [\mathbf{D}\mathbf{M}_m^{\gamma_m}(0) + \mathbf{C}][\mathbf{A} + \mathbf{B}\mathbf{M}_m^{\gamma_m}(0)]^{-1}, \quad (9.108)$$

where the  $\mathbf{A}$ ,  $\mathbf{B}$ ,  $\mathbf{C}$ , and  $\mathbf{D}$  matrices in Eq. (9.108) are given by matrix products of the propagation and transmission matrices in the 4x4 matrix form

$$\begin{bmatrix} \mathbf{A} & \mathbf{B} \\ \mathbf{C} & \mathbf{D} \end{bmatrix} = \begin{bmatrix} \mathbf{A}_m^t & \mathbf{B}_m^t \\ \mathbf{C}_m^t & \mathbf{D}_m^t \end{bmatrix} \begin{bmatrix} \mathbf{A}_m^d & \mathbf{B}_m^d \\ \mathbf{C}_m^d & \mathbf{D}_m^d \end{bmatrix} \quad (9.109)$$

This result can be obtained directly by placing Eq. (9.103) into Eq. (9.106) and rearranging the result in the form of Eq. (9.108).

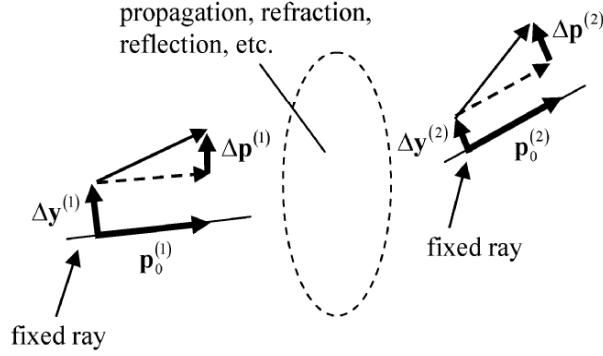


**Fig. 9.13.** Paraxial rays before and after a given wave process such as propagation, refraction, reflection, etc.

Obviously, this process can be continued for any additional materials and interfaces present. For example, in going from medium 1 to medium  $M+1$  through  $M$  interfaces we can relate the  $\mathbf{M}$  matrix in the final material at a distance  $s_{M+1}$  from the  $M$ th interface directly to the starting  $\mathbf{M}$  matrix values in medium 1 in terms of “global” matrices  $\mathbf{A}^G, \mathbf{B}^G, \mathbf{C}^G, \mathbf{D}^G$  as

$$\mathbf{M}_{M+1}^{\gamma_{M+1}}(s_{M+1}) = [\mathbf{D}^G \mathbf{M}_1^{\gamma_1}(0) + \mathbf{C}^G] [\mathbf{A}^G + \mathbf{B}^G \mathbf{M}_1^{\gamma_1}(0)]^{-1}, \quad (9.110)$$

where  $\mathbf{A}^G, \mathbf{B}^G, \mathbf{C}^G, \mathbf{D}^G$  are given by products of all the contributing propagation and transmission matrices, i.e.

$$\begin{bmatrix} \mathbf{A}^G & \mathbf{B}^G \\ \mathbf{C}^G & \mathbf{D}^G \end{bmatrix} = \begin{bmatrix} \mathbf{A}_{M+1}^d & \mathbf{B}_{M+1}^d \\ \mathbf{C}_{M+1}^d & \mathbf{D}_{M+1}^d \end{bmatrix} \begin{bmatrix} \mathbf{A}_M^t & \mathbf{B}_M^t \\ \mathbf{C}_M^t & \mathbf{D}_M^t \end{bmatrix} \cdot \begin{bmatrix} \mathbf{A}_M^d & \mathbf{B}_M^d \\ \mathbf{C}_M^d & \mathbf{D}_M^d \end{bmatrix} \cdots \begin{bmatrix} \mathbf{A}_1^d & \mathbf{B}_1^d \\ \mathbf{C}_1^d & \mathbf{D}_1^d \end{bmatrix}. \quad (9.111)$$

Thus, all the  $\mathbf{M}$  matrices appearing in either Eq. (9.100a) or Eq. (9.100b) can be obtained via the appropriate matrix multiplications of the type shown in Eq. (9.111). To compute the Gaussian beam in the final medium we need (1) the propagation and transmission/reflection  $\mathbf{A}, \mathbf{B}, \mathbf{C}, \mathbf{D}$  matrices for a specified set of wave types and wave paths, (2) the plane wave transmission/reflection coefficients that allow us to compute the  $\mathbf{T}_m^{\gamma_{m+1}; \gamma_m}$  matrices, and (3) the velocity,  $V_1^{\gamma_1}(0) \mathbf{d}_i^{\gamma_1}$ , and phase matrix,  $\mathbf{M}_1^{\gamma_1}(0)$ , of the Gaussian beam at the starting point in the first medium.

The **A**, **B**, **C**, **D** matrices for propagation, transmission, and reflection appear in Eqs. (9.103) and (9.106) in exactly the same form because these equations are the consequence of some fundamental paraxial ray theory relations. To see this, consider a wave front moving in space defined at a given time by the function  $T(\mathbf{x}) = \text{constant}$ . As a simple example a plane wave traveling in the **e**-direction with wave speed  $c$  has the wave front  $T(\mathbf{x}) = T_0 + \mathbf{e} \cdot \mathbf{x} / c = T_0 + \mathbf{p} \cdot \mathbf{x}$ , with  $T_0$  a constant and  $\mathbf{p} \equiv \mathbf{e} / c$  the slowness vector. For a more general curved wave front we define the components of the slowness vector by  $p_i = \partial T / \partial x_i$ . We also define the curvatures of the wave front as the second derivatives,  $\hat{M}_{ij} \equiv \partial^2 T / \partial x_i \partial x_j$  or, equivalently,  $\hat{M}_{ij} = \partial p_i / \partial x_j$ . In a homogeneous, isotropic medium the wave propagation rays are just straight lines along the slowness vector so we can examine a given fixed ray and some general process such as propagation, refraction, reflection, etc. as shown in Fig. 9.13. After such a process the slowness vector may be changed from  $\mathbf{p}_0^{(1)}$  to  $\mathbf{p}_0^{(2)}$ . On a nearby (paraxial) ray, defined by its displacement vector  $\Delta \mathbf{y}$  relative to our fixed ray, both the displacement and slowness will change during the process under consideration from  $\Delta \mathbf{y}^{(1)}$  to  $\Delta \mathbf{y}^{(2)}$  and  $\mathbf{p}_0^{(1)} + \Delta \mathbf{p}^{(1)}$  to  $\mathbf{p}_0^{(2)} + \Delta \mathbf{p}^{(2)}$ , respectively. Since we are considering small deviations in going from the fixed ray to the nearby paraxial ray, we expect that these changes are linearly related to one another, i.e.

$$\begin{Bmatrix} \Delta \mathbf{y}^{(2)} \\ \Delta \mathbf{p}^{(2)} \end{Bmatrix} = \begin{bmatrix} \mathbf{A} & \mathbf{B} \\ \mathbf{C} & \mathbf{D} \end{bmatrix} \begin{Bmatrix} \Delta \mathbf{y}^{(1)} \\ \Delta \mathbf{p}^{(1)} \end{Bmatrix}, \quad (9.112)$$

where **A**, **B**, **C**, **D** are the “proportionality constants”. To first order we also relate the changes in the slowness vectors to changes in the displacement vectors through wave front curvatures **M**, i.e.

$$\begin{aligned} \Delta \mathbf{p}^{(1)} &= \mathbf{M}_1 \Delta \mathbf{y}^{(1)} \\ \Delta \mathbf{p}^{(2)} &= \mathbf{M}_2 \Delta \mathbf{y}^{(2)}. \end{aligned} \quad (9.113)$$

If we use the expression for  $\Delta \mathbf{p}^{(1)}$  in Eq. (9.113) in the expression for  $\Delta \mathbf{y}^{(2)}$  in Eq. (9.112) we obtain

$$\Delta \mathbf{y}^{(2)} = \mathbf{A} \Delta \mathbf{y}^{(1)} + \mathbf{B} \mathbf{M}_1 \Delta \mathbf{y}^{(1)}. \quad (9.114)$$

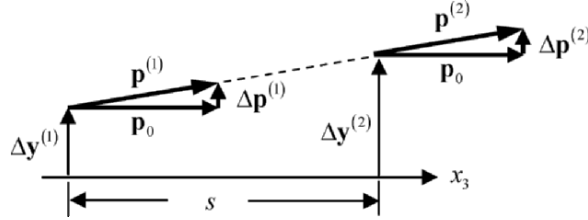


**Fig. 9.14.** Propagation of a paraxial ray.

Similarly, placing  $\Delta \mathbf{p}^{(2)}$  from Eq. (9.113) into the expression for  $\Delta \mathbf{p}^{(2)}$  in Eq. (9.112) gives

$$\mathbf{M}_2 \Delta \mathbf{y}^{(2)} = \mathbf{C} \Delta \mathbf{y}^{(1)} + \mathbf{D} \mathbf{M}_1 \Delta \mathbf{y}^{(1)} \quad (9.115)$$

so that combining Eqs. (9.114) and (9.115) yields

$$\mathbf{M}_2 (\mathbf{A} + \mathbf{B} \mathbf{M}_1) \Delta \mathbf{y}^{(1)} = (\mathbf{C} + \mathbf{D} \mathbf{M}_1) \Delta \mathbf{y}^{(1)}. \quad (9.116)$$

Since Eq. (9.116) must be true for all  $\Delta \mathbf{y}^{(1)}$  in the neighborhood of the fixed ray, we find

$$\mathbf{M}_2 = [\mathbf{D} \mathbf{M}_1 + \mathbf{C}] [\mathbf{A} + \mathbf{B} \mathbf{M}_1]^{-1}, \quad (9.117)$$

which has the same structure of Eqs. (9.103) and (9.106). Thus, our Gaussian beam relations can be thought of as the extension of ordinary paraxial ray theory relations for a real wave front curvature matrix  $\mathbf{M}$  to a complex-valued  $\mathbf{M}$  matrix that defines a Gaussian beam and we can view our  $\mathbf{A}$ ,  $\mathbf{B}$ ,  $\mathbf{C}$ ,  $\mathbf{D}$  matrices as the terms defining the paraxial changes of the ray parameters in Eq. (9.112). For example, consider propagation through a distance  $s$  at a wave speed  $c$  along a paraxial ray which is near a fixed ray along the  $x_3$ -axis as shown in Fig. 9.14. It is easy to see that  $\Delta \mathbf{p}^{(2)} = \Delta \mathbf{p}^{(1)}$  and  $\Delta \mathbf{y}^{(2)} = \Delta \mathbf{y}^{(1)} + s c \Delta \mathbf{p}^{(1)}$ , where we have  $\Delta \mathbf{p}^{(1)} = (\Delta p_1^{(1)}, \Delta p_2^{(1)})$  and  $\Delta \mathbf{p}^{(2)} = (\Delta p_1^{(2)}, \Delta p_2^{(2)})$ , and that this leads directly to

$$\begin{Bmatrix} \Delta y_2 \\ \Delta p_2 \end{Bmatrix} = \begin{bmatrix} \mathbf{I} & (s c) \mathbf{I} \\ 0 & \mathbf{I} \end{bmatrix} \begin{Bmatrix} \Delta y_1 \\ \Delta p_1 \end{Bmatrix}, \quad (9.118)$$

which corresponds to the propagation  $\mathbf{A}$ ,  $\mathbf{B}$ ,  $\mathbf{C}$ ,  $\mathbf{D}$  matrices defined by Eq. (9.104). Another more mathematical way to view the  $\mathbf{ABCD}$  parameters



is to recognize them as components of a *propagator matrix*. See Cerveny [9.2], who defines such propagator matrices and discusses their properties in detail.

Equations (9.108) and (9.110) can also lead to a further simplification of the amplitude terms in Eq. (9.100b), which can be rewritten in terms of propagation **A**, **B** matrices as

$$\begin{aligned} \mathbf{v}_{M+1}^{\alpha;(y)} &= \frac{1}{\sqrt{\det[\mathbf{A}_{M+1}^d + \mathbf{B}_{M+1}^d \mathbf{M}_{M+1}^\alpha(0)]}} \\ &\cdot \left[ \prod_{m=M}^1 \frac{\mathbf{T}_m^{\gamma_{m+1};\gamma_m}}{\sqrt{\det[\mathbf{A}_m^d + \mathbf{B}_m^d \mathbf{M}_m^{\gamma_m}(0)]}} \right] \\ &\cdot V_1^{\gamma_1}(0) \mathbf{d}_1^{\gamma_1} \exp \left[ i\omega \sum_{m=1}^{M+1} \frac{s_m}{c_m^{\gamma_m}} + i \frac{\omega}{2} \mathbf{y}^T \hat{\mathbf{M}}_{M+1}^\alpha(s_{M+1}) \mathbf{y} \right]. \end{aligned} \quad (9.119)$$

To reduce this equation, we first use Eq. (9.106) and the fact that  $\mathbf{B}_m^t = \mathbf{0}$  to show directly that

$$[\mathbf{A}_{m+1}^d + \mathbf{B}_{m+1}^d \mathbf{M}_{m+1}^{\gamma_{m+1}}(0)] = [\mathbf{A}' + \mathbf{B}' \mathbf{M}_m^{\gamma_m}(s_m)] [\mathbf{A}_m^t]^{-1}, \quad (9.120)$$

where

$$\begin{bmatrix} \mathbf{A}' & \mathbf{B}' \\ \mathbf{C}' & \mathbf{D}' \end{bmatrix} = \begin{bmatrix} \mathbf{A}_{m+1}^d & \mathbf{B}_{m+1}^d \\ \mathbf{C}_{m+1}^d & \mathbf{D}_{m+1}^d \end{bmatrix} \begin{bmatrix} \mathbf{A}_m^t & \mathbf{B}_m^t \\ \mathbf{C}_m^t & \mathbf{D}_m^t \end{bmatrix}. \quad (9.121)$$

Also, using Eq. (9.103) it follows that

$$[\mathbf{A}' + \mathbf{B}' \mathbf{M}_m^{\gamma_m}(s_m)] = [\mathbf{A}^G + \mathbf{B}^G \mathbf{M}_m^{\gamma_m}(0)] [\mathbf{A}_m^d + \mathbf{B}_m^d \mathbf{M}_m^{\gamma_m}(0)]^{-1}, \quad (9.122)$$

where  $\mathbf{A}^G, \mathbf{B}^G$  are global matrices that combine the effects of propagation in media  $m$  and  $m+1$  and transmission across the  $m$ -th interface, i.e.

$$\begin{bmatrix} \mathbf{A}^G & \mathbf{B}^G \\ \mathbf{C}^G & \mathbf{D}^G \end{bmatrix} = \begin{bmatrix} \mathbf{A}_{m+1}^d & \mathbf{B}_{m+1}^d \\ \mathbf{C}_{m+1}^d & \mathbf{D}_{m+1}^d \end{bmatrix} \begin{bmatrix} \mathbf{A}_m^t & \mathbf{B}_m^t \\ \mathbf{C}_m^t & \mathbf{D}_m^t \end{bmatrix} \begin{bmatrix} \mathbf{A}_m^d & \mathbf{B}_m^d \\ \mathbf{C}_m^d & \mathbf{D}_m^d \end{bmatrix}. \quad (9.123)$$

Then from Eq. (9.120) and Eq. (9.122) we obtain

$$\begin{aligned} &[\mathbf{A}_{m+1}^d + \mathbf{B}_{m+1}^d \mathbf{M}_{m+1}^{\gamma_{m+1}}(0)] \\ &= [\mathbf{A}^G + \mathbf{B}^G \mathbf{M}_m^{\gamma_m}(0)] [\mathbf{A}_m^d + \mathbf{B}_m^d \mathbf{M}_m^{\gamma_m}(0)]^{-1} [\mathbf{A}_m^t]^{-1}. \end{aligned} \quad (9.124)$$

Now, examine two successive square root terms in Eq. (9.119) for medium  $m$  and  $m+1$ , i.e.

$$I = \frac{1}{\sqrt{\det[\mathbf{A}_{m+1}^d + \mathbf{B}_{m+1}^d \mathbf{M}_{m+1}^{\gamma_{m+1}}(0)]}} \frac{1}{\sqrt{\det[\mathbf{A}_m^d + \mathbf{B}_m^d \mathbf{M}_m^{\gamma_m}(0)]}}. \quad (9.125)$$

Placing Eq. (9.124) into Eq. (9.125) we find

$$I = \frac{\sqrt{\det[\mathbf{A}_m^t]}}{\sqrt{\det[\mathbf{A}^G + \mathbf{B}^G \mathbf{M}_m^{\gamma_m}(0)]}}. \quad (9.126)$$

Since this same process can be repeated for all the other pairs of amplitude terms in Eq. (9.119), that equation reduces to

$$\begin{aligned} \mathbf{v}_{M+1}^{\alpha;(y)} &= \frac{\tilde{\mathbf{T}}_M}{\sqrt{\det[\mathbf{A}^G + \mathbf{B}^G \mathbf{M}_1^{\gamma_1}(0)]}} V_1^{\gamma_1}(0) \mathbf{d}_1^{\gamma_1} \\ &\cdot \exp \left[ i\omega \sum_{m=1}^{M+1} \frac{s_m}{c_m^{\gamma_m}} + i \frac{\omega}{2} \mathbf{y}^T \hat{\mathbf{M}}_{M+1}^{\alpha}(s_{M+1}) \mathbf{y} \right], \end{aligned} \quad (9.127)$$

where  $\mathbf{A}^G, \mathbf{B}^G$  are now the global matrices going from medium 1 to medium  $M+1$  and

$$\tilde{\mathbf{T}}_M = \prod_{m=M}^1 \mathbf{T}_m^{\gamma_{m+1}; \gamma_m} \sqrt{\det[\mathbf{A}_m^t]}. \quad (9.128)$$

Equation (9.127) is in the form identical in structure to that of a Gaussian beam propagating in a single medium. Thus, use of the **ABCD** matrices can simplify our multiple media problems to an equivalent single medium expression. However, to use Eq. (9.127) one must be able to correctly evaluate the square root of the amplitude in that equation and at present we do not have a direct way to do that evaluation. The difficulty lies in that  $\mathbf{A}^G, \mathbf{B}^G$  are no longer positive, real, diagonal matrices as they are for a single medium, so that the signs of the imaginary parts of the eigenvalues of  $\mathbf{M}_1^{\gamma_1}$  are affected in a manner that is difficult to explicitly define. Thus, while Eq. (9.127) is in the most compact form possible either Eq. (9.100a) or Eq. (9.100b) appear to be needed in actual calculations. Of course the **ABCD** matrices can be conveniently used to obtain all the terms needed in those equations.

## 9.5 Multi-Gaussian Transducer Beam Modeling

We have seen in the previous sections how to analytically determine a Gaussian beam after it has propagated in multiple media and interacted with multiple interfaces. In NDE applications the value of those results would be limited if Gaussian beams were the only types of wave fields that we could consider since most ultrasonic transducers do not generate Gaussian-shaped beams. Instead, we would like to be able to model the wave fields from piston transducers. This is possible since in a seminal 1988 paper Wen and Breazeale showed that one can synthesize the sound beam from a circular piston transducer radiating into water using the superposition of as few as ten Gaussian beams [9.8]. On the face of a transducer of radius  $a$  located on the plane  $x_3 = 0$  (and radiating into the region  $x_3 > 0$ ) they let the normalized velocity field be given by a sum of Gaussians in the form

$$\frac{\mathbf{v}^p(x_1, x_2, 0, \omega)}{v_0(\omega)} = \sum_{r=1}^{10} A_r \mathbf{d}^p \exp(-B_r \rho^2 / a^2), \quad (9.129)$$

where  $\rho^2 = x_1^2 + x_2^2$ ,  $v_0(\omega)$  is the constant velocity on the transducer surface, and  $\mathbf{d}^p = \mathbf{e}_3 = (0, 0, 1)$ . These ten Gaussians will generate ten Gaussian beams having starting values of  $[V_1^p(0)]_r, [\mathbf{M}_1^p(0)]_r$  ( $r = 1, \dots, 10$ ) given by

$$\begin{aligned} [V_1^p(0)]_r &= A_r v_0(\omega) \\ [\mathbf{M}_1^p(0)]_r &= \begin{bmatrix} \frac{iB_r}{c_{p1}D_R} & 0 \\ 0 & \frac{iB_r}{c_{p1}D_R} \end{bmatrix}, \end{aligned} \quad (9.130)$$

where  $D_R = k_{p1}a^2/2$  is the *Rayleigh distance*.  $A_r, B_r$  are complex-valued expansion coefficients that need to be determined to match the velocity field on the face of the transducer. For a circular planar piston transducer of radius  $a$ , the normalized velocity field in the  $x_3$ -direction,  $v_3/v_0$ , is given by the *circ function*, where

$$\frac{v_3(x_1, x_2, 0, \omega)}{v_0(\omega)} = \begin{cases} 1 & \rho^2 / a^2 < 1 \\ 0 & \text{otherwise} \end{cases} \quad (9.131)$$

$$\equiv \text{circ}(\rho^2 / a^2).$$

To obtain the  $A_r, B_r$  coefficients, Wen and Breazeale minimized an objective function,  $J$ , given by

$$J(A_r, B_r) = \int_0^\infty \left[ \text{circ}(\rho^2 / a^2) - \sum_{r=1}^{10} A_r \exp(-B_r \rho^2 / a^2) \right]^2 d\rho \quad (9.132)$$

and they published the ten coefficients that they obtained. Although this is a non-linear optimization problem that is rather computationally intensive, once the  $A_r, B_r$  coefficients are calculated, they can be stored in a look-up table and used to synthesize the wave field in very complex problems simply by adding up the ten contributing Gaussians. Thus, we can use Eq. (9.100a) to write down the wave field from a piston transducer, after multiple propagations and interface interactions, in the form of a multi-Gaussian beam model, where

$$\mathbf{v}_{M+1}^{\alpha(y)} = \sum_{r=1}^{10} \frac{\sqrt{\det[\mathbf{M}_{M+1}^\alpha(s_{M+1})]_r}}{\sqrt{\det[\mathbf{M}_{M+1}^\alpha(0)]_r}} \left[ \prod_{m=M}^1 \mathbf{T}_m^{\gamma_{m+1}, \gamma_m} \frac{\sqrt{\det[\mathbf{M}_m^{\gamma_m}(s_m)]_r}}{\sqrt{\det[\mathbf{M}_m^{\gamma_m}(0)]_r}} \right] \quad (9.133)$$

$$\cdot [V_1^{\gamma_1}(0)]_r \mathbf{d}_1^{\gamma_1} \exp \left[ i\omega \sum_{m=1}^{M+1} \frac{s_m}{c_m^{\gamma_m}} + i \frac{\omega}{2} \mathbf{y}^T [\hat{\mathbf{M}}_{M+1}^\alpha(s_{M+1})]_r \mathbf{y} \right].$$

The success of this approach, of course, relies on how well the ten coefficients used here do represent a piston transducer wave field. Tests of the ten Wen and Breazeale coefficients show that they do a remarkably effective job of reproducing the piston transducer wave field to within the limits of the paraxial approximation. This means that they are accurate at distances of approximately one transducer diameter or greater from the transducer face. This can be easily tested by examining the normalized pressure wave field of the multi-Gaussian beam model for a single fluid medium given by

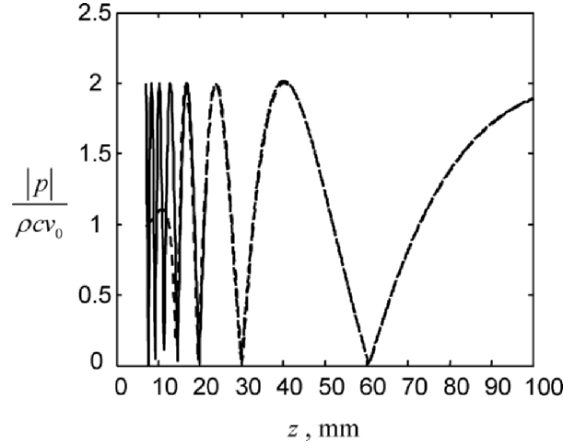


**Fig. 9.15.** The magnitude of the normalized on-axis pressure for a 6 mm radius piston transducer radiating into water at 5 MHz modeled by the Rayleigh-Sommerfeld integral (solid line) and by a superposition of ten Gaussian beams which are defined by the ten coefficients of Wen and Breazeale.

$$\frac{p(x_1, x_2, x_3, \omega)}{\rho_1 c_{p1} v_0(\omega)} = \sum_{r=1}^{10} \frac{A_r}{1 + iB_r x_3 / D_R} \exp(ik_{p1} x_3) \cdot \exp \left[ i\omega \left( \frac{1}{2} \mathbf{x}^T [\mathbf{M}_1^p(x_3)]_r \mathbf{x} \right) \right], \quad (9.134)$$

where

$$[\mathbf{M}_1^p(x_3)]_r = \begin{bmatrix} \frac{iB_r / c_{p1} D_R}{1 + iB_r x_3 / D_R} & 0 \\ 0 & \frac{iB_r / c_{p1} D_R}{1 + iB_r x_3 / D_R} \end{bmatrix}. \quad (9.135)$$

Comparisons of Eq. (9.134) can be made with the exact solution obtained from the Rayleigh-Sommerfeld equation for any point in the transducer wave field but the results are very similar to comparisons done for on-axis wave fields, where we can write down an exact solution analytically (Eq. (9.8)). Figure 9.15 shows such an on-axis comparison for a 6 mm radius planar piston transducer radiating into water at 5 MHz. The multi-Gaussian beam model accurately models the on-axis near-field of the transducer down to approximately 15 mm from the transducer face.

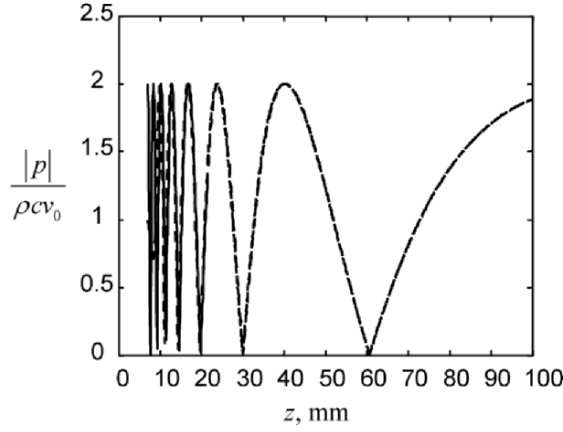


**Fig. 9.16.** The magnitude of the normalized on-axis pressure for a 6 mm radius piston transducer radiating into water at 5 MHz modeled by the Rayleigh-Sommerfeld integral (solid line) and by a superposition of fifteen Gaussian beams defined by the fifteen “optimized” coefficients of Wen and Breazeale.

In a subsequent paper, Wen and Breazeale obtained even better results with a slightly larger number of optimized coefficients [9.9]. They used the normalized exact on-axis pressure,  $\tilde{p}_{exact}$ , defined as

$$\tilde{p}_{exact}(x_3, \omega) = \frac{p(0, 0, x_3, \omega)}{\rho_1 c_{p1} v_0} = \exp(ik_{p1} x_3) - \exp(ik_{p1} \sqrt{a^2 + x_3^2}) \quad (9.136)$$

and a 15 term multi-Gaussian beam model for this same wave field:

$$\tilde{p}_{MG}(x_3, \omega) = \sum_{r=1}^{15} \frac{A_r}{1 + iB_r x_3 / D_R} \exp(ik_{p1} x_3) \quad (9.137)$$

to define a modified objective function

$$J(A_r, B_r) = \int_0^\infty \left[ \text{circ}(\rho^2 / a^2) - \sum_{r=1}^{15} A_r \exp(-B_r \rho^2 / a^2) \right]^2 d\rho \quad (9.138)$$

$$+ \lambda_w \int_{z_1}^{z_2} \left[ |\tilde{p}_{exact}(x_3, \omega)| - |\tilde{p}_{MG}(x_3, \omega)| \right]^2 dx_3$$

where  $\lambda_w$  is a constant to weigh the on-axis matching conditions relative to the boundary matching conditions and  $z_1$  and  $z_2$  are near field limit values that define the range where matching to the on-axis field is to take

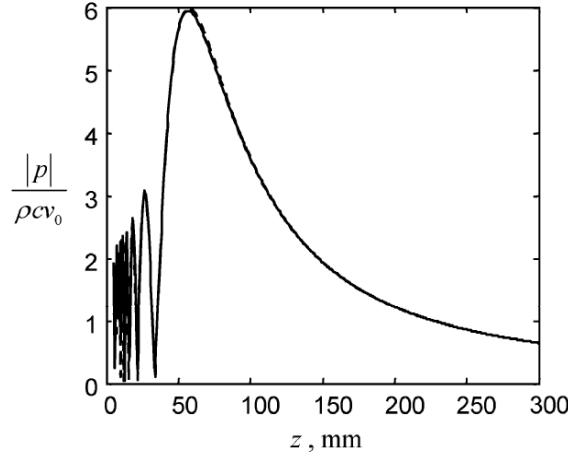


**Fig. 9.17.** The magnitude of the on-axis pressure for a 6 mm radius, 76 mm focal length spherically focused transducer radiating into water at 5MHz. Solid line – exact O’Neil theory, dashed line – multi-Gaussian beam model.

place. Fig. 9.16 shows the results of using these 15 optimized coefficients to calculate the on-axis field where now the multi-Gaussian beam model is accurate at distances from the transducer of approximately 10 mm or greater, matching the exact on-axis behavior for two additional near-field oscillations. These fifteen optimized coefficients are listed both in [9.9] and [9.10] and generated by a MATLAB function `gauss_c15` given in Chapter 12 (Code Listing 12.2).

One of the nice properties of this multi-Gaussian beam model is that one can also model focused transducers by a simple modification of the  $B_r$  coefficient. As shown in Chapter 8, focusing in the paraxial approximation can be modeled by including a complex exponential term with a quadratic spatial variation for the velocity field over the face of a planar transducer. For a spherically focused circular transducer of radius  $a$  and geometrical focal length,  $F$ , this corresponds to specifying the velocity field at the transducer as

$$\frac{v_3(x_1, x_2, 0, \omega)}{v_0(\omega)} = \text{circ}(\rho^2 / a^2) \exp(-ik_{p1}\rho^2 / 2F). \quad (9.139)$$

Since we can view our multi-Gaussian beam model as approximating this *circ* function in the form

$$\text{circ}(\rho^2 / a^2) = \sum_{r=1}^{10} A_r \exp(-B_r \rho^2 / a^2) \quad (9.140)$$

Eq. (9.139) shows that to include the effects of spherical focusing we need only to modify the  $B_r$  coefficients for the circular planar transducer case by making the replacement

$$B_r \rightarrow B_r + \frac{ik_p a^2}{2F} \quad (9.141)$$

Figure 9.17 shows the on-axis wave field predicted by a multi-Gaussian beam model obtained in this fashion for a 6 mm radius, 76 mm focal length transducer radiating into water at 5 MHz and the corresponding on-axis field obtained from the O'Neil model (Eq. (8.33)). It can be seen that there is very little discernable difference between the two results.

Recently, Ding et al. [9.11] made a clever use of the *circ* function and the ten coefficients of Wen and Breazeale to model rectangular piston transducers. For a rectangular piston transducer with sides of lengths  $(2a_1, 2a_2)$  in the  $(x_1, x_2)$  directions, respectively, the normalized velocity field on the transducer face is given by

$$\begin{aligned} \frac{v_3(x_1, x_2, 0, \omega)}{v_0(\omega)} &= \begin{cases} 1 & |x_1 / a_1| < 1, |x_2 / a_2| < 1 \\ 0 & \text{otherwise} \end{cases} \\ &= \text{circ}(x_1^2 / a_1^2) \text{circ}(x_2^2 / a_2^2) \end{aligned} \quad (9.142)$$

so if we use Eq. (9.140) in product form we have

$$\begin{aligned} &\text{circ}(x_1^2 / a_1^2) \text{circ}(x_2^2 / a_2^2) \\ &= \sum_{r=1}^{10} \sum_{q=1}^{10} A_r A_q \exp \left[ i\omega \left( \frac{1}{2} \mathbf{x}^T [\mathbf{M}_1^p(0)]_{rq} \mathbf{x} \right) \right] \\ &= \sum_{r=1}^{10} \sum_{q=1}^{10} A_r A_q \exp \left[ -B_r x_1^2 / a_1^2 - B_q x_2^2 / a_2^2 \right], \end{aligned} \quad (9.143)$$

where  $\mathbf{x}^T = (x_1, x_2)$  and



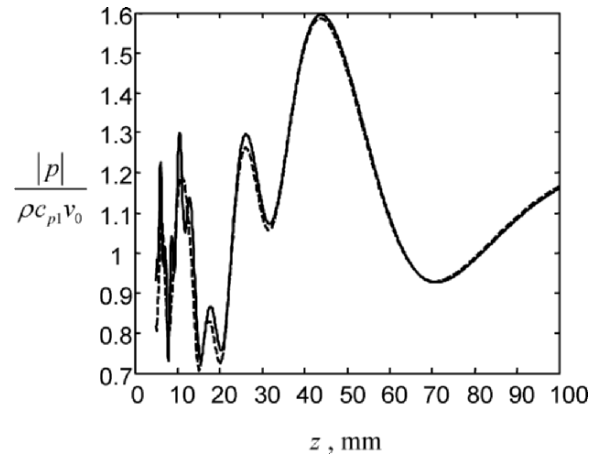


**Fig. 9.18.** Magnitude of the on-axis pressure for a 12x6 mm rectangular piston transducer radiating into water at 5 MHz using the Rayleigh-Sommerfeld integral (solid line) and a multi-Gaussian beam model based on the ten coefficients of Wen and Breazeale.

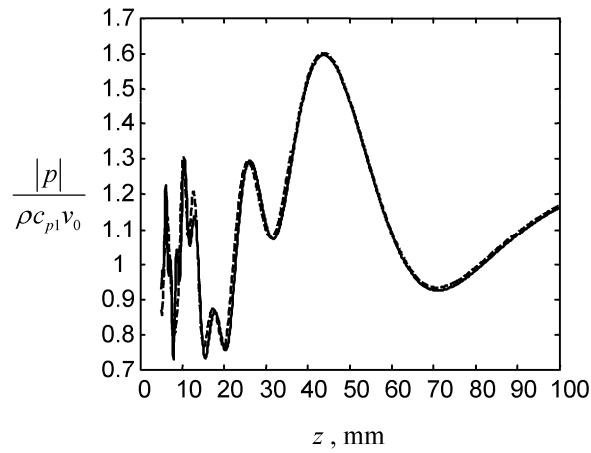


**Fig. 9.19.** Magnitude of the on-axis pressure for a 12x6 mm rectangular piston transducer radiating into water at 5 MHz using the Rayleigh-Sommerfeld integral (solid line) and a multi-Gaussian beam model based on the fifteen “optimized” coefficients of Wen and Breazeale.

$$[\mathbf{M}_i^p(0)]_{rq} = \begin{bmatrix} \frac{iB_r}{c_{p1}D_{R1}} & 0 \\ 0 & \frac{iB_q}{c_{p1}D_{R2}} \end{bmatrix} \quad (9.144)$$

and  $D_{R1} = k_{p1}a_1^2/2$ ,  $D_{R2} = k_{p1}a_2^2/2$ .

Using these results we can write a multi-Gaussian beam model for a rectangular planar piston transducer radiating through multiple media and interacting with multiple interfaces as

$$\begin{aligned} \mathbf{v}_{M+1}^{\alpha;(y)} = & \sum_{r=1}^{10} \sum_{q=1}^{10} [V_1^{\gamma_1}(0)]_{rq} \mathbf{d}_1^{\gamma_1} \frac{\sqrt{\det[\mathbf{M}_{M+1}^\alpha(s_{M+1})]_{rq}}}{\sqrt{\det[\mathbf{M}_{M+1}^\alpha(0)]_{rq}}} \\ & \cdot \left[ \prod_{m=M}^1 \mathbf{T}_m^{\gamma_{m+1};\gamma_m} \frac{\sqrt{\det[\mathbf{M}_m^{\gamma_m}(s_m)]_{rq}}}{\sqrt{\det[\mathbf{M}_m^{\gamma_m}(0)]_{rq}}} \right] \\ & \cdot \exp \left[ i\omega \sum_{m=1}^{M+1} \frac{s_m}{c_m^{\gamma_m}} + i \frac{\omega}{2} \mathbf{y}^T [\hat{\mathbf{M}}_{M+1}^\alpha(s_{M+1})]_{rq} \mathbf{y} \right], \end{aligned} \quad (9.145)$$

where  $[V_1^{\gamma_1}(0)]_{rq} = A_r A_q v_0(\omega)$ .

For a rectangular transducer radiating into a single fluid medium, the normalized on-axis pressure of this multi-Gaussian beam model is given by

$$\begin{aligned} \frac{p(0,0,x_3,\omega)}{\rho_1 c_{p1} v_0(\omega)} = & \sum_{r=1}^{10} \sum_{q=1}^{10} \frac{A_r}{\sqrt{1+iB_r x_3/D_{R1}}} \frac{A_q}{\sqrt{1+iB_q x_3/D_{R2}}} \\ & \cdot \exp(ik_{p1} x_3). \end{aligned} \quad (9.146)$$

This model has been compared to a highly accurate numerical integration of the Rayleigh-Sommerfeld equation for a 12x6 mm rectangular transducer ( $a_1 = 6 \text{ mm}$ ,  $a_2 = 3 \text{ mm}$ ) radiating into water at 5 MHz as shown in Fig. 9.18. It can be seen from that figure that the multi-Gaussian beam model agrees well with the “exact” results at distances of 15 mm or greater from the transducer. Although the 15 optimized coefficients of Wen and Breazeale were specifically optimized for the circular transducer, it has been found that those coefficients also improve the results for rectangular transducers.

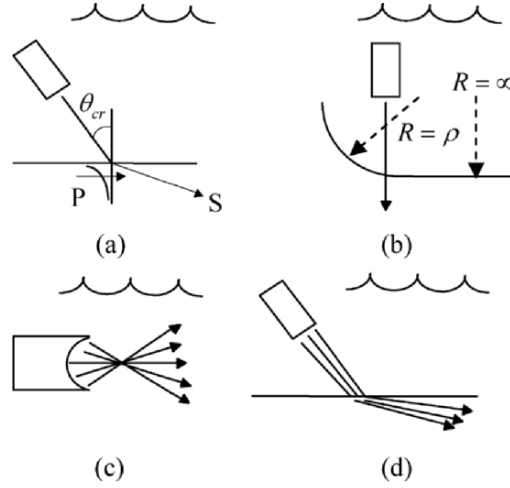


**Fig. 9.20.** Conditions under which the paraxial approximation can fail include: **(a)** transmission through an interface near a critical angle, **(b)** inspection through a surface with rapidly changing curvature, **(c)** for highly focused transducers, and **(d)** near grazing incidence to a surface.

For example, Figure 9.19 shows that using these 15 coefficients the multi-Gaussian beam model matched the exact results to within a distance less than 6 mm for the same transducer considered in Fig. 9.18.

As in the circular transducer case, it is easy to add focusing to the multi-Gaussian beam rectangular transducer model. For example, in the case of a bi-cylindrically focused rectangular transducer with geometrical focal lengths  $(F_1, F_2)$  in the  $(x_1, x_2)$  directions, respectively, one again merely has to modify the  $B_r, B_q$  coefficients by making the replacements

$$\begin{aligned} B_r &\rightarrow B_r + \frac{ik_{p1}a_1^2}{2F_1} \\ B_q &\rightarrow B_q + \frac{ik_{p1}a_2^2}{2F_2}. \end{aligned} \quad (9.147)$$

It is possible to use the Wen and Breazeale coefficients to also model elliptical-shaped piston transducers [9.11]. There are also other fitting methods that can be used to obtain the coefficients such as the k-space method of Sha et al. [9.12]. However, the 15 optimized coefficients of

Wen and Breazeale generate about as accurate a wave field that is possible within the paraxial approximation [9.13].

Because the multi-Gaussian beam model relies on the paraxial approximation being valid, there are a number of testing situations where the model can degrade or fail. We have already seen that in the very near field the paraxial approximation will fail. Since most ultrasonic testing is not done under such very near field conditions, this limitation of the paraxial models may not be of practical importance. However, the breakdown of the paraxial approximation can also occur under other testing conditions. Figure 9.20 (a) shows the case when a transducer radiates through a planar fluid-solid interface at an angle near the first critical angle. In this case the waves reaching the point in the solid may be at very small angles relative to the central ray but the paraxial approximation can fail because, near a critical angle, the transmission coefficient that defines the amplitude of the waves in the solid varies rapidly for even small angular changes and such variations are neglected when paraxial beam models are used to treat transmission through interfaces (recall that we used the transmission coefficient along a central ray only in considering the interactions with an interface). Figure 9.20 (b) shows the inspection of a surface at the intersection of a fillet and a plane surface. In this case the surface curvature,  $R$ , changes abruptly from  $R = \infty$  to  $R = \rho$  at the intersection and the paraxial approximation fails because of this rapid change of the surface curvature. Figure 9.20 (c) illustrates the case of a very tightly focused transducer. The paraxial approximation also fails in this case as the waves reaching the focus do not travel in approximately the same direction as required by that approximation. Finally, Fig. 9.20 (d) shows the case of the inspection through a plane interface at high angles or near grazing incidence on the interface. The paraxial approximation can fail in this case also since it cannot capture the strong beam distortions present at these high angles and there may be other waves besides bulk P-waves and S-waves (head waves, surface waves, etc.) present near the interface that are not considered by our beam model. Fortunately, many of these special testing situations are not encountered in practice so that the multi-Gaussian beam model is a fast and powerful tool and gives accurate results in many cases.

## 9.6 References

- 9.1 Siegman AE (1986) Lasers. University Science Books, Mill Valley, CA
- 9.2 Cerveny V (2001) Seismic ray theory. Cambridge University Press, Cambridge, United Kingdom

- 9.3 Jeffreys A (1995) Handbook of mathematical formulas and integrals. Academic Press, San Diego, CA, p 48
- 9.4 Heyman E, Felsen LB (2001) Gaussian beam and pulsed-beam dynamics: complex-source and complex-spectrum formulations within and beyond paraxial asymptotics. *J. Opt. Soc. Am.* 18: 1588-1611
- 9.5 Korn GA, Korn TM (1968) Mathematical handbook for scientists and engineers. McGraw-Hill Book Co., New York, NY
- 9.6 Cerveny V, Psencik I. (1983) Gaussian beams and paraxial ray approximation in three-dimensional inhomogeneous elastic media. *Journal of Geophysics* 53: 1-15
- 9.7 Goldsmith PF (1998) Quasioptical systems. IEEE Press, Piscataway, NJ
- 9.8 Wen JJ, Breazeale MA (1988) A diffraction beam field expressed as the superposition of Gaussian beams. *J. Acoust. Soc. Am.* 83: 1752-1756
- 9.9 Wen JJ, Breazeale MA (1990) Computer optimization of the Gaussian beam description of an ultrasonic field. In: Lee D, Cakmak A, Vichnevetsky R. (eds) Computational acoustics: scattering, Gaussian beams, and aeroacoustics, Vol. 2. Elsevier Science Publishers, Amsterdam, The Netherlands, pp 181-196
- 9.10 Huang D, Breazeale MA (1999) A Gaussian finite-element method for description of sound diffraction. *J. Acoust. Soc. Am.* 106: 1771-1781
- 9.11 Ding D, Zhang Y, Liu J (2003) Some extensions of the Gaussian beam expansion: radiation fields of rectangular and elliptical transducers. *J. Acoust. Soc. Am.* 113: 3043-3048
- 9.12 Sha K, Yang J, Gan WS (2003) A complex virtual source approach for calculating the diffraction beam field generated by a rectangular planar source. *IEEE Trans. on Ultrasonics, Ferroelectrics, and Frequency Control* 50: 890-896
- 9.13 Kim HJ, Schmerr LW, Sedov A (2006) Generation of the basis sets for multi-Gaussian ultrasonic beam models – an overview. *J. Acoust. Soc. Am.* 119: 1971-1978

## 9.7 Exercises

1. Equation (9.134) gives the normalized pressure of a circular planar piston transducer as computed by a multi-Gaussian beam model. Write a MATLAB function that takes as its inputs the frequency,  $f$ , the wave speed of the water (in m/sec), the radius,  $a$ , of the transducer (in mm), and the distances  $(x_1, x_2, x_3)$  (in mm) and computes this normalized pressure in the water. Use the fifteen Gaussian beam coefficients (instead of the ten terms indicated in Eq. (9.134)) which can be obtained from the MATLAB function `gauss_c15`. Verify that your function produces the magnitude of the on-axis pressure plot shown in Fig. 9.16 for a 6 mm radius transducer

radiating into water at 5 MHz. For this same transducer, plot the magnitude of the normalized pressure versus  $x_2$  for  $x_1 = 0, x_3 = 60$  mm.

2. Modify the MATLAB function written for the circular planar transducer of exercise 1 to model a spherically focused transducer of focal length,  $R$ , using the relationship of Eq. (9.141). Verify that your function produces the magnitude of the on-axis pressure plot for a 6 mm radius, 76 mm focal length focused transducer radiating into water at 5 MHz (Fig. 9.17). For this same transducer plot the magnitude of the cross-axis normalized pressure at the geometrical focal length  $x_3 = 76$  mm and compare this pressure to the exact result given by Eq. (8.42).

3. The multi-Gaussian beam model for the normalized pressure of a planar rectangular transducer radiating into a fluid is given from Eq. (9.145) (for 15 Gaussian beams) by

$$\frac{p(x_1, x_2, x_3, \omega)}{\rho_1 c_{p1} v_0(\omega)} = \sum_{r=1}^{15} \sum_{q=1}^{15} \frac{A_r}{\sqrt{1 + iB_r x_3 / D_{R1}}} \frac{A_q}{\sqrt{1 + iB_q x_3 / D_{R2}}} \cdot \exp(ik_{p1} x_3) \exp \left[ i\omega \left( \frac{1}{2} \mathbf{x}^T [\mathbf{M}_1^p(x_3)]_{rq} \mathbf{x} \right) \right],$$

where  $\mathbf{x}^T = (x_1, x_2)$  and

$$[\mathbf{M}_1^p(x_3)]_{rq} = \begin{bmatrix} \frac{iB_r / c_{p1} D_{R1}}{1 + iB_r x_3 / D_{R1}} & 0 \\ 0 & \frac{iB_q / c_{p1} D_{R2}}{1 + iB_q x_3 / D_{R2}} \end{bmatrix}.$$

Write a MATLAB function that takes as its inputs the frequency,  $f$ , the wave speed of the water (in m/sec), the half-lengths  $(a_1, a_2)$  of the transducer (in mm), and the distances  $(x_1, x_2, x_3)$  (in mm) and computes this normalized pressure in the water. The Gaussian beam coefficients can be obtained from the MATLAB function `gauss_c15`. Verify that your function produces the magnitude of the on-axis pressure plot shown in Fig. 9.19 for a 12x6 mm transducer radiating into water at 5 MHz. Note that the half-lengths of the two sides are given here by  $a_1 = 6$  mm,  $a_2 = 3$  mm. For this same transducer, plot the magnitude of the normalized

pressure versus distance  $x_2$  for  $x_1 = 0$ ,  $x_3 = 20$  mm and versus distance  $x_1$  for  $x_2 = 0$ ,  $x_3 = 20$  mm.

4. Modify the MATLAB function of exercise 3 to model a cylindrically focused rectangular transducer where the focusing is in the  $x_1 - x_3$  plane, by using a relationship similar to Eq.(9.141), i.e.

$$B_r \rightarrow B_r + \frac{ik_{p1}a_1^2}{2F_1}$$

$$B_q \text{ unchanged.}$$

The Gaussian beam coefficients can again be obtained from the MATLAB function gauss\_c15. Plot the magnitude of the on-axis pressure for a 12x6 mm transducer with cylindrical focal length  $F_1 = 80$  mm radiating into water at 5 MHz.

5. Rewrite Eq. (9.134) for the normalized pressure wave field of a circular planar transducer radiating into a fluid (using 15 Gaussian beams) in terms of  $(x, y, z)$  coordinates as

$$\frac{p(x, y, z, \omega)}{\rho_1 c_{p1} v_0(\omega)} = \sum_{r=1}^{15} \frac{A_r}{1 + iB_r z / D_R} \cdot \exp(ik_{p1}z) \exp\left[i\omega \left(\frac{1}{2} \mathbf{x}^T [\mathbf{M}_1^p(z)]_r \mathbf{x}\right)\right],$$

where  $\mathbf{x}^T = (x, y)$  and

$$[\mathbf{M}_1^p(z)]_r = \begin{bmatrix} \frac{iB_r / c_{p1} D_R}{1 + iB_r z / D_R} & 0 \\ 0 & \frac{iB_r / c_{p1} D_R}{1 + iB_r z / D_R} \end{bmatrix}.$$

This expression can also be written as a quasi-plane wave in the form

$$p(x, y, z, \omega) = \rho_1 c_{p1} v_0 \exp(ik_{p1}z) C(a, x, y, z, \omega),$$

where  $C$  is a diffraction coefficient. We can use the paraxial approximation discussion of Chapter 8 (see section 8.5) and quickly obtain a multi-Gaussian beam model for a planar, circular P-wave transducer radiating at normal

incidence to a fluid-solid interface by writing the normalized pressure in the solid in the quasi-plane wave form

$$\frac{p(x, y, z, \omega)}{\rho_1 c_1 v_0} = \exp(ik_{p1}z_1 + ik_{p2}z_2) C(a, x, y, \tilde{z}, \omega),$$

where  $\tilde{z} = z_1 + z_2 \frac{c_{p2}}{c_{p1}}$  and  $(z_1, z_2)$  are the distances traveled normal to the interface in the water and solid, respectively, as discussed in Chapter 8. Note that this normalized pressure is also the same as the normalized velocity  $v_z / v_0$  (see Eq. (8.25)).

Use this result to write a MATLAB function that implements a multi-Gaussian beam model for a transducer radiating at normal incidence to a fluid-solid interface and evaluate and plot the magnitude of the normalized on-axis pressure for a 6.35 mm radius transducer radiating at 5 MHz through a water-aluminum interface where the water path distance  $z_1 = 50.8$  mm, and the metal path distance,  $z_2$ , ranges from zero to 25.4 mm.